Constraining $f(\mathcal{R})$ gravity by Pulsar SAX J1748.9-2021 observations

Gamal G. L. Nashed *
Centre for Theoretical Physics, The British University, P.O. Box 43, El Sherouk City, Cairo 11837, Egypt.

Salvatore Capozziello †
Dipartimento di Fisica E. Pancini, Universit'a di Napoli Federico II Complesso Universitario di Monte Sant Angelo, Edificio G, Via Cinthia, I-80126, Napoli, Italy, Scuola Superiore Meridionale, Largo S. Marcellino 10, I-80138, Napoli, Italy, and Istituto Nazionale di Fisica Nucleare (INFN), Sez. di Napoli Complesso Universitario di Monte Sant Angelo, Edificio G, Via Cinthia, I-80126, Napoli, Italy.

(Dated: May 17, 2024)

We discuss spherically symmetric dynamical systems in the framework of a general model of $f(\mathcal{R})$ gravity, i.e. $f(\mathcal{R}) = \mathcal{R}e^{\zeta\mathcal{R}}$, where ζ is a dimensional quantity in squared length units [L^2]. We initially assume that the internal structure of such systems is governed by the Krori-Barua ansatz, alongside the presence of fluid anisotropy. By employing astrophysical observations obtained from the pulsar SAX J1748.9-2021, derived from bursting X-ray binaries located within globular clusters, we determine that ζ is approximately equal to ± 5 km^2. In particular, the model can create a stable configuration for SAX J1748.9-2021, encompassing its geometric and physical characteristics. In $f(\mathcal{R})$ gravity, the Krori-Barua approach links p_r and p_t, which represent the components of the pressures, to (ρ), representing the density, semi-analytically. These relations are described as $p_r \approx v_r^2(\rho - \rho_I)$ and $p_t \approx v_t^2(\rho - \rho_{II})$. Here, the expression v_r and v_t represent the radial and tangential sound speeds, respectively. Meanwhile, ρ_I pertains to the surface density and ρ_{II} is derived using the parameters of the model. Notably, within the frame of $f(\mathcal{R})$ gravity where ζ is negative, the maximum compactness, denoted as C, is inherently limited to values that do not exceed the Buchdahl limit. This contrasts with general relativity or with $f(\mathcal{R})$ with positive ζ, where C has the potential to reach the limit of the black hole asymptotically. The predictions of such model suggest a central energy density which largely exceeds the saturation of nuclear density, which has the value $\rho_{\rm nuc} = 3 \times 10^{14}$ g/cm^3. Also, the density at the surface ρ_I surpasses $\rho_{\rm nuc}$. We obtain the relation between mass and radius represent it graphically, and show that it is consistent with other observational data.

arXiv:2405.09590v1 [gr-qc] 15 May 2024

* nashed@bue.edu.eg
† capozziello@na.infn.it

I. INTRODUCTION

Experiments measuring the perihelion advance of Mercury, the gravitational Doppler effect, and light deflection, all of which are used to evaluate the accuracy of Einstein's general relativity (GR) at solar-system scales, have demonstrated exceptionally high precision, as reported in [1]. Additionally, GR has undergone tests in extreme gravitational conditions: For example, detecting gravitational waves produced by the collision of compact celestial objects [2, 3]. As a consequence, GR has risen as the most successful and widely accepted theory for explaining gravitational phenomena. However, Einstein's theory presents shortcomings at UV scales for the lack of a viable quantum gravity, and at IR scales because significant issues related to observed Universe remain unanswered. In fact, to account for cosmic acceleration within the framework of GR, we need to introduce dark energy, which is an unusual form of matter-energy characterized by a substantial negative pressure. Furthermore, a huge amount of dark matter is required to address dynamics of cosmic structures like galaxies and clusters of galaxies. In both cases, at the moment, there is no answer at fundamental level explaining such a dark side.

In recent decades, numerous alternative gravitational theories have arisen, aiming to explain the expansion that accelerates Universe and cosmic structure dynamics. Specifically, GR can be modified or extended at UV and IR scales in order to achieve a comprehensive explanation of the early inflationary era involving dark energy, at late epochs. citeStarobinsky:1980te, Capozziello:2002rd, Carroll:2003wy, Hu:2007nk, Nojiri:2006ri, Amendola:2006we, Appleby:2007vb, Odintsov:2020nwm, Koyama:2015vza,Nojiri:2003ft, Nojiri:2007cq, Cognola:2007zu, Oikonomou:2020qah, Oikonomou:2020oex.

A straightforward method for improving GR is substituting the scalar curvature $\mathcal{R}$ with $f\mathcal{R}$, giving rise to what is known as $f(\mathcal{R})$ gravity. Related models have been explored as potential explanations for dynamics of both early and late Universe. Comprehensive reviews on this topic are [18–23]. Conversely, at astrophysical scales, modifications of GR impact also the characteristics of compact stars. In fact, in the context of $\mathcal{R}^2$ gravity, commonly known as the Starobinsky model [4], and using a non-perturbative methodology, there is a significant increase in the maximum mass of compact stars on the diagram of mass and radius, primarily attributable to the quadratic term [24–32]. Researches indicate that in the context of $\mathcal{R}$-squared gravity, the secondary component of the GW190814 event, as reported by the LIGO-Virgo collaboration in [33], can be effectively characterized as a NS [28–30, 34]. In particular, the physical properties of neutron stars (NSs) have been examined both for non-rotating [35] and rotating [36] systems, within the context of $\mathcal{R}^2$ gravity coupled with an axion scalar field. In [37] thoroughly review stellar structure models within modified gravity theories, and develop in metric and metric-affine approaches.

It has been shown in Ref. [38] that the flat rotation curves of galaxies can be explained by only small departures from GR. Specifically, they found that a gravitational Lagrangian taking the form $f(\mathcal{R}) \propto \mathcal{R}^{1+\zeta_1}$ represents a relatively natural modification of Einstein gravity, with the dimensionless parameter ζ_1 being communicated in terms of the tangential speed. In addition, there has been interest in this power-law $f(\mathcal{R})$ model lately as a potential solution to the clustered galactic dark matter issue [39], where the parameter ζ_1 is constrained to be of the order of 10^{-6}. In this context, Ref. [39] was used to calculate the light deflection angle using the rotational velocity profile of typical nearby galaxies in the gravitational background of $\mathcal{R}^{1+\zeta_1}$. Additional investigations of the consequences of $f(\mathcal{R})$ power law can be found in. [40–46].

Conversely, it has been demonstrated that the parameter ζ_1, in the context of $\mathcal{R}^{1+\zeta_1}$ theory, possesses a substantial influence on the mass and radius plots of isotropic NSs [28, 47].Although isotropic perfect fluids are commonly used to describe the matter inside compact stars, there are good reasons to take anisotropies in extremely dense matter into consideration [48–64]. These studies demonstrate that the existence of anisotropy can either raise or decrease the maximal-mass threshold, thereby offering the potential to attain more massive compact stars that align with astronomical observations.

Folomeev conducted a comprehensive investigation of the impact of anisotropies on the internal structure of NSs, employing a completely autonomous non-perturbative method inside the Starobinsky mode. This study considered three distinct types of realistic equations of state (EoSs) [65]. The incorporation of anisotropic pressure has been shown to facilitate the utilization of stiffer equations of state (EoSs) to represent configurations that meet observational criteria effectively. Furthermore, Ref.[66] delved into the exploration of anisotropic quark stars within $\mathcal{R}$-squared gravity, and more recently, in [67] examined anisotropic compact stars in relation to theories of higher-order curvature such as $f(\mathcal{R})$.According to [70–73], a study of compact anisotropic structures in the Starobinsky form and within generalised modified gravity has been conducted. The gravitational collapse of an anisotropic system with heat flow was investigated in Ref. [74] using the Karmarkar condition and taking a logarithmic modification of the standard Starobinsky model into account. For a comparative analysis of self-consistent charged anisotropic spheres in an embedded spacetime framework with the Karmarkar condition applied, see Ref. [75].

To the best of our information, there is no investigation into anisotropic compact stars within the framework of the $\mathcal{R}e^{\zeta\mathcal{R}}$ gravity model. As we will see below, this $f(\mathcal{R})$ model is particularly suitable to investigate small deviations with respect to GR. With this objective at the forefront, we aim to formulate the equations that govern the stellar

structure in this gravitational model and explore the impact of compact star anisotropy. For this goal,We'll make use of the so-called Krori-Barua (KB) ansatz to close the system of differential equations.

The structure of the paper is the following: In Section II, we offer a concise overview of $f(\mathcal{R})$ theory. In Section III, we introduce the specific $f(\mathcal{R})$ model, namely $f(\mathcal{R}) = \mathcal{R}e^{\zeta\mathcal{R}}$, and derive the form of the system of differential equations, which is presented in detail in the Supplementary Material. For the sake of computational convenience, we employ the KB ansatz and deduce the expressions for density, radial pressure, and tangential pressure, as detailed in the Supplementary Material. Utilizing matching conditions, we determine the model parameters.

In Section IV, pulsar's mass and radius from astrophysical observations of SAX J1748.9-2021 are used to derive constraints on the model parameter ζ. In Section V,e examine the physical quantity deviations from GR and provide numerical results. Finally, in Section VI, we summarize our results. It is worth noticing that we use geometrical units $G = 1 = c$ and the spacetime signature $(-,+,+,+)$ for our computations. However, final results are reported in physical units.

II. THE THEORETICAL FRAMEWORK

A. $f(R)$ gravity in metric formalism

In this section, we provide a concise overview of $f(\mathcal{R})$ gravity adopting the metric formalism. The action is

$$S = \frac{1}{2\kappa^2}\int d^4x\sqrt{-g}f(\mathcal{R}) + S_m\,. \tag{1}$$

In this study, the Ricci scalar in this case is denoted by $\mathcal{R}$, the matter action is denoted by S_m, and the determinant of $g_{\mu\nu}$ is g. The equation of motion is obtained as follows when we change the action with respect to the metric:

$$f_{\mathcal{R}}\mathcal{R}_{\mu\nu} - \frac{1}{2}g_{\mu\nu}f - \nabla_\mu\nabla_\nu f_{\mathcal{R}} + g_{\mu\nu}\Box f_{\mathcal{R}} = \kappa^2 T_{\mu\nu}\,. \tag{2}$$

The gravitational coupling is $\kappa^2 = \frac{8\pi G}{c^4}$, with G the Newton constant and c the speed of light. Additionally, we have the matter energy-momentum tensor denoted as $T_{\mu\nu}$.

Furthermore, we define $f_{\mathcal{R}}$ as the derivative of $f(\mathcal{R})$ with respect to $\mathcal{R}$, and the covariant derivative ∇_μ connected to the metric's Levi-Civita connection. Here $\Box$ is the d'Alembert operator. Finally, $\mathcal{R}_{\mu\nu}$ is the Ricci tensor.

In GR, $\mathcal{R}$ for a stellar fluid is defined by its energy density and pressure, which are $\mathcal{R} = -8\pi T$, where $T = g_{\mu\nu}T^{\mu\nu}$. However, in $f(\mathcal{R})$ gravity, both the metric tensor $g_{\mu\nu}$ and the Ricci scalar $\mathcal{R}$ are non-trivial. Consequently, $\mathcal{R}$ is now prescribed by a second order differential equation which can be derived from Eq. (2) as:

$$3\Box f_{\mathcal{R}}(\mathcal{R}) + \mathcal{R}f_{\mathcal{R}}(\mathcal{R}) - 2f(\mathcal{R}) = \kappa^2 T\,, \tag{3}$$

which means that in comparison to GR, where $T = 0$ leads to $\mathcal{R} = 0$, if nonlinear functions of $\mathcal{R}$ are taken into account, additional curvature components must also be taken into consideration even when standard matter is absent. In other words, a curvature fluid has to be taken into account [5, 20].

B. Spherical symmetry

To investigate the internal composition of a stellar in an equilibrium, we analyze a spherically symmetric system where the spacetime is characterized by the metric

$$ds^2 = -e^\mu dt^2 + e^\nu dr^2 + r^2(d\theta^2 + \sin^2\theta d\phi^2)\,, \tag{4}$$

where the spacetime is given by Schwarzschild-like coordinates $x^\alpha = (t, r, \theta, \phi)$. Here, μ and ν are function of r only. We assume that the distribution of stellar matter is an anisotropic perfect fluid, i.e., it can be prescribed by:

$$T_{\alpha\beta} = (\rho + p_t)u_\alpha u_\beta + p_t g_{\alpha\beta} - \sigma k_\alpha k_\beta\,, \tag{5}$$

where u^α is the four-velocity of the fluid with the normalization condition $u_\alpha u^\alpha = -1$; k^α is a unit radial four-vector satisfying the condition $k_\alpha k^\alpha = 1$. Here, the energy density is represented by ρ, the tangential pressure by p_t, the radial pressure by p_r, and the anisotropy factor by $\sigma \equiv p_t - p_r$.

According to the above metric, we can express u^α as $e^{-\mu}\delta^\alpha_t$, and k^α as $e^{-\nu}\delta^\alpha_r$. As a result, the energy-momentum tensor (5) trace has the following form:

$$T = -\rho + 3p_r + 2\sigma\,. \tag{6}$$

The conservation law of momentum and energy can be obtained from the divergence of Equation (5) which yields:

$$\nabla_\nu T_r{}^\nu = p_r' + (\rho + p_r)\mu' - \frac{1}{r}\sigma = 0\,. \tag{7}$$

Here $'$ denotes the derivative W.r.t.r. Furthermore, it is

$$\Box f_{\mathcal{R}} = \frac{1}{\sqrt{-g}}\partial_\mu\left[\sqrt{-g}\partial^\mu f_{\mathcal{R}}\right] = e^{-\nu}\left[\left(\frac{1}{r} + \mu' - \nu'\right) f_{\mathcal{R}}' + f_{\mathcal{R}}''\right]. \tag{8}$$

Hence, the energy-momentum tensor (5) and the line element (4) provide, from the field equations (2), the following non-zero components:

$$-\frac{f_{\mathcal{R}}}{r^2} + \frac{f_{\mathcal{R}}}{r^2}\frac{d}{dr}\left(re^{-\nu}\right) + \frac{1}{2}(\mathcal{R}f_{\mathcal{R}} - f) + e^{-\nu}\left[\left(\frac{2}{r} - \nu'\right) f_{\mathcal{R}}' + f_{\mathcal{R}}''\right] = -8\pi\rho, \tag{9}$$

$$-\frac{f_{\mathcal{R}}}{r^2} + \frac{f_{\mathcal{R}}}{e^\nu}\left(\frac{\mu'}{r} + \frac{1}{r^2}\right) + \frac{1}{2}(\mathcal{R}f_{\mathcal{R}} - f) + e^{-\nu}\left(\frac{2}{r} + \mu'\right) f_{\mathcal{R}}' = 8\pi p_r, \tag{10}$$

$$\frac{f_{\mathcal{R}}}{r^2}\left[1 + e^{-\nu}(r\nu' - r\mu' - 1)\right] - \frac{1}{2}f + e^{-\nu}\left[\left(\frac{1}{r} + \mu' - \nu'\right) f_{\mathcal{R}}' + f_{\mathcal{R}}''\right] = 8\pi p_t\,. \tag{11}$$

The equation governing the evolution of scalar curvature (3) now becomes

$$3e^{-\nu}\left[\left(\frac{1}{r} + \mu' - \nu'\right) f_{\mathcal{R}}' + f_{\mathcal{R}}''\right] = \kappa(p_r + 2p_t - \rho) + 2f - \mathcal{R}f_{\mathcal{R}}\,. \tag{12}$$

III. THE $f(\mathcal{R})$ GRAVITY MODEL

Let us now adopt the following $f(\mathcal{R})$ model:

$$f(\mathcal{R}) = \mathcal{R}e^{\zeta\mathcal{R}}\,, \tag{13}$$

where ζ represents a parameter with dimensions [L^2], with L a length. When the dimensional parameter ζ is set to zero, the standard Einstein GR is recovered. Conversely, for small non-zero ζ, the expression can be recast as

$$f(\mathcal{R}) = \mathcal{R} + \zeta\mathcal{R}^2 + \frac{1}{2}\zeta^2\mathcal{R}^3\cdots\,. \tag{14}$$

For these reasons, Eq. (13) is a general $f(\mathcal{R})$ model capable of representing both small and large deviations with respect to GR.

Upon inserting the expression for $f(\mathcal{R})$ as provided in Eq. (13) into Eqs. (9) through (11), we derive a lengthy system, which is reported in the Supplementary Material. One can readily observe that when considering $\zeta = 0$, the matter density and pressure components undergo modifications and ultimately converge to the GR solution, as demonstrated in previous works [76, 77]. Nevertheless, the system in Eqs. (1), (2), and (3), presented in the Supplementary Material, encompasses five unknown functions necessitating the imposition of two extra constraints to define it. A possible approach is assuming suitable EoS to establish connections between radial and tangential pressures and density. However, this approach may not be practical due to the presence of a challenging fourth-order differential equation within the system.

An alternative approach is considering reasonable assumptions for the metric potentials $\mu(r)$ and $\nu(r)$. We will adopt this method and consider the so called Krori-Barua (KB) spacetime to investigate stellar models in the frame of $f(\mathcal{R})$ theory of gravity.

A. The Krori-Barua framework

Let us introduce the metric potentials of the KB form, as described in [78]:

$$\mu(r) = s_0(r/R)^2 + s_1, \qquad \nu(r) = s_2(r/R)^2\,, \tag{15}$$

here, R represents the radius of the star, and the parameters $[s_0, s_1, s_2]$ are dimensionless and can be determined by satisfying junction conditions. Equation (15) ensures a singularity-free solution across the whole interior of the star. The ansatz of KB has been applied in diverse gravitational theories, including GR. However, in the present investigation, we employ observational constraints derived from the pulsar *SAX J1748.9-2021* to estimate the model parameter ζ. By employing Eq. (15) and Eqs. (1), (2), and (3) presented in the Supplementary Material, we can expressed the components of the energy-momentum tensor.

Moreover, we present the notion of the anisotropic which is defined as $F_a = \frac{2\sigma}{r}$, which arises due to the pressure difference, equivalently represented by anisotropy $\sigma = p_t - p_r$. Significantly, the anisotropy becomes zero at the central point. In the strong anisotropy situation, $\sigma > 0$, for $0 < r \leq R$, it necessitates that $p_t > p_r$ across the star's interior. Conversely, in mild anisotropy case, i.e., $\sigma < 0$, it requires that $p_r > p_t$ throughout the interior of the star.

B. Matching Conditions

For a stellar system, we can suppose that the vacuum solutions of GR correspond to those of $f(\mathcal{R})$ given in Eq. (13). This means that the external solution simply aligns with Schwarzschild spacetime. Thus, we choose to represent vacuum space as:

$$ds^2 = -\left(1 - \frac{2GM}{c^2 r}\right)c^2 dt^2 + \left(1 - \frac{2GM}{c^2 r}\right)^{-1} dr^2 + d\Omega^2, \qquad \text{where} \quad d\Omega^2 = r^2(d\theta^2 + \sin^2\theta d\phi^2)\,. \tag{16}$$

In this context, M describes star's mass. Applying the junction conditions we get:

$$\mu_{(\mathrm{r=R})} = \ln(1 - C), \qquad \nu_{(r=R)} = -\ln(1 - C)\,, \qquad a\mathrm{nd} \qquad p_{r\,(r=R)=0}\,, \tag{17}$$

with C represents compactness described as:

$$C = \frac{2GM}{c^2 R}\,. \tag{18}$$

By adopting Eq. (15) and using p_t from Eqs. (4) in the Supplementary Material, we can establish the specified surface limits. This allows us to express the model parameters $[s_0, s_1, s_2]$ in terms of $\zeta_1 = \frac{\zeta}{R^2}$ and C.The pulsar mass and radius can be constrained by astrophysical observations, which, in turn, determine the compactness; consequently, the next step is observationally constraining the parameter ζ_1.

IV. CONSTRAINTS AND STABILITY CONSIDERATIONS FROM *S*AX J1748.9-2021 OBSERVATIONS

In this section, we utilize observational limitations, with a specific focus on M and R of stellar SAX J1748.9-2021, to determine the value of the parameter ζ_1 in the frame of $f(\mathcal{R})$ theory of gravity. Furthermore, we subject the obtained solution to a thorough evaluation of its stability based on different physical limits. As mentioned earlier in the Introduction, accurate observational data plays a vital role in limiting the parameter space. To begin, our selection criteria are presented for the pulsar SAX J1748.9-2021 aiming to limit $f(\mathcal{R})$ theory of gravity. This choice is based on the availability of time-resolved spectroscopic data from EXO 1745-248 during thermonuclear bursts, which has yielded precise measurements for the pulsar ($M = 1.81 \pm 0.3 M_\odot$) and ($R = 11.7 \pm 1.7$ km) [79, 80]. By leveraging M and R of the pulsar SAX J1748.9-2021, we narrow ζ_1 of $f(\mathcal{R})$ model. This parameter space comprises the set of parameters $[\zeta,\ s_0,\ s_1,\ s_2]$.

A. The material component

Referring to equations presented in the Supplementary Material, and taking into account numerical estimation for the model parameters, we generate plots illustrating ρ, p_r and p_t as functions dependent on r. These plots are reported

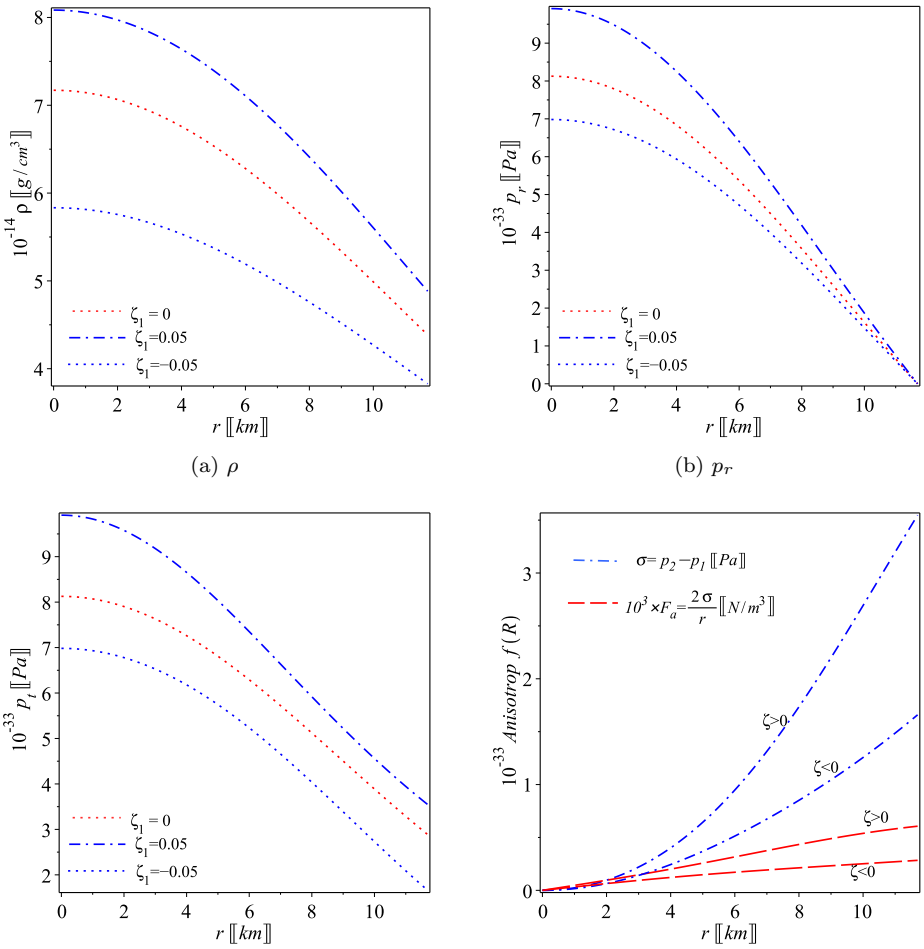

(a) ρ (b) p_r (c) p_t (d) Δ

Figure 1. With regard to the pulsar's matter sector SAX J1748.9-2021, Figs. (a) through (c) represent the profiles of density as well as p_r and p_t pressure components, presented in the Supplementary Material, for different values of ζ_1, specifically $\zeta_1 = 0,\ \pm 0.05$. The figures confirm that ρ, p_r and p_t remain limited throughout the interior of the stellar and exhibit a monotonic decrease towards its surface. In Fig. (d), we present the distribution of anisotropy, denoted as $\sigma(r)$, within the stellar for varying values of ζ_1, specifically $\zeta_1 = 0,\ \pm 0.05$. Notably, the anisotropy vanishes at the central point where $p_t = p_r$, while it assumes positive values elsewhere.

in Figures 1(a)–(c). The density and pressure profiles clearly adhere to the stability criteria within the material sector, which we are going to discuss below. They reach their maximum values at the core, maintain positivity, and are free of singularities throughout the star's interior. They exhibit a monotonic decrease towards the star surface. Furthermore, we generate a figure representing the difference between pressures (i.e., anisotropy$\equiv \Delta$), as illustrated in plot 1(d). Such graph demonstrates that Δ adheres the requirement of stability, as it reaches zero at the core and steadily grows in a monotonic way towards the star surface. It's important to note that the strong anisotropy criteria, as analyzed in this study, introduces an extra positive force, proportional to σ/r, which impacts the material's overall performance and influences hydrodynamic equilibrium. Such force acts against the force of gravity, playing a pivotal role in adjusting the size of the star, which enables it to support a larger mass compared to scenarios with isotropy or mild anisotropy. A more thorough explanation of this impact can be found in Subsection IV G.

It is worth providing numerical values for physical quantities associated with the pulsar SAX J1748.9-2021, as predicted by the current model.
For instance, with $\zeta_1 = 0.05$, the core density is approximately $\rho_{\rm core} \approx 8.08 \times 10^{14}$ g/cm^3, that roughly 3 times $\rho_{\rm nuc}$, and both $p_{r(\rm core)}$ and $p_{t(\rm core)}$, are approximately 9.91×10^{33} dyn/cm^2. At the star boundary, we show $\rho_I = 4.88 \times 10^{14}$ g/cm^3, that ≈ 1.8 times $\rho_I = 4.88 \times 10^{14}$ g/cm^3, $p_{r(r=R)} = 0$ dyn/cm^2, and $p_{t(r=R)} \approx 3.55 \times 10^{33}$ dyn/cm^2.

When $\zeta_1 = -0.05$, $\rho_{\rm core} \approx 5.83 \times 10^{14}$ g/cm^3, that 2.16 times $\rho_I = 4.88 \times 10^{14}$ g/cm^3, and pressure components at the center are approximately 7×10^{33} dyn/cm^2. At boundary, we get $\rho_I = 3.83 \times 10^{14}$ g/cm^3, that ≈ 1.4 times $\rho_I = 4.88 \times 10^{14}$ g/cm^3, $p_{r(r=R)} = 0$ dyn/cm^2, $p_{t(r=R)} \approx 1.66 \times 10^{33}$ dyn/cm^2.

In this context, it is noteworthy that the stellar model under consideration doesn't eliminate the chance that the pulsar *SAX J1748.9-2021* has a core composed by neutrons. As indicated in Section III, the KB ansatz (15) has been employed as an alternative to EoSs in order to close the system presented in the Supplementary Material. Furthermore, we demonstrate that the KB efficiently establishes relations between the components of the energy-momentum tensor. In order to realize this, we present $\xi := r/R$ and subsequently expand the power series of Eqs. (4) presented in the Supplementary Material up to $O(\xi^4)$. It is evident that the procedure leads to the following relations:

$$p_r(\rho) \approx a_1\rho + a_2\,, \qquad p_t(\rho) \approx a_3\rho + a_4\,. \tag{19}$$

The constants denoted as $a_1, ..., a_4$ are entirely determined in the model parameter space, which is $[\zeta_1, s_0, s_1, s_2]$, as detailed in the Supplementary Material. Remarkably, we can express the equations above in a more physically meaningful way as follows:

$$p_r(\rho) \approx v_r^2(\rho - \rho_I)\,, \qquad p_t(\rho) \approx v_t^2(\rho - \rho_{II})\,. \tag{20}$$

In this context, we can interpret the following physical parameters as follows: v_r^2 represents the sound of speed in the r direction, ρ_I is the density (specifically, the surface density ρ_I satisfying the boundary condition $p_r(\rho_I) = 0$), v_t^2 denotes the speed of sound in the tangential direction, and ρ_{II} represents another density. It is worth noticing that the condition $p_r(\rho_I) = 0$ applies to ρ_I, but not necessarily to ρ_{II}, since p_t may not vanish on the surface. These parameters encompass two special cases: For hadron matter, the equation of state (EoS), which is maximally compact, where $v_r^2{=}c^2$, and the EoS based on the MIT which represents the bag model of quark matter, where $v_r^2{=}c^2/3$. For instance, when $\zeta_1 = 0.05$, using Eqs. (4) as detailed in the Supplementary Material, we obtain the following values: $v_r^2 = a_1 \approx 0.43c^2$, $v_t^2 = a_3 \approx 0.337c^2$, $\rho_I = -a_2/a_1 = 5.9 \times 10^{14}$ g/cm^3, and $\rho_{II} = -a_4/a_3 \approx 4.3 \times 10^{14}$ g/cm^3. Likewise, for $\zeta_1 = -0.05$, we obtain the following values: $v_r^2 \approx 0.385c^2$, $v_t^2 \approx 0.29c^2$, $\rho_I = 3.9 \times 10^{14}$ g/cm^3, and $\rho_{II} \approx 4.1 \times 10^{14}$ g/cm^3.

B. The geometric component

The function of the gravitational redshift, corresponding to our ansatz is as follows:

$$Z(r) = \frac{1}{\sqrt{-g_{tt}}} - 1 = \frac{1}{\sqrt{e^{s_0(r/R)^2+s_1}}} - 1\,. \tag{21}$$

We creat a figure of the pulsar's SAX J1748.9-2021 redshift function as reported in Fig. 2(a). In the GR case, i.e., $\zeta_1 = 0$, Z at the core is approximately $Z(0) \approx 0.675$, and at the boundary $Z_R \approx 0.35$. If $\zeta_1 = -0.05$, Z at $r = 0$ yields $Z(0) \approx 0.646$ less than GR. Importantly, this value remains below the maximum limit $Z_s = 2$, as discussed in [81–84]. Likewise, for $\zeta_1 = 0.05$, we observe that the upper limit of Z at the center is $Z(0) \approx 0.69$ which remains below the maximum limit.

It effectively conveys that the redshift distributions in the frame of $f(\mathcal{R})$ satisfy stability limits in both cases discussed. It effectively communicates that the value of $Z > 0$ and has a finite value within the star's interior, decreasing monotonically towards the boundary, and has a positive redshift and its first derivative is negative as demonstrated in Fig. 2(a).

C. Limits on the mass radius relation from SAX J1748.9-2021 observations

In the following analysis, we utilize the value of mass and the value of radius evaluated from observation of the stellar *SAX J1748.9-2021*, which are reported as $M = 1.81 \pm 0.3 M_\odot$ and $R = 11.7 \pm 1.7$ km according to [79], to impose constraints on the parameter ζ_1 within the framework of $f(R)$ theory. Mass distribution, within the radius of the stellar is given as:

$$m(r) = 4\pi \int_0^r \rho(\eta)\eta^2 d\eta\,. \tag{22}$$

Recalling the density profile presented in the Supplementary Material, for the $f(\mathcal{R}) = \mathcal{R}e^{\zeta\mathcal{R}}$, we show in the Fig. 2(b) that:

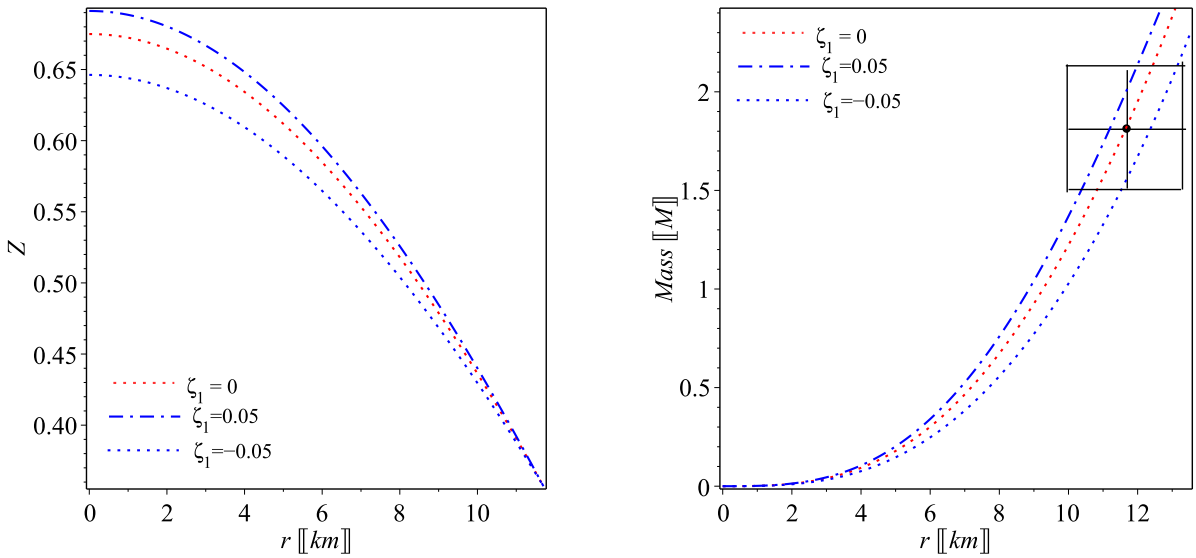

(a) Redshift

(b) Mass function

Figure 2. In all the figures presented in this study, we have consistently employed identical numerical values assigned to the model parameters. (a): This graph displays the redshift function (21) for various cases, including $\zeta_1 = 0 \ \pm 0.05$. In all scenarios, the high redshift is observed at the core with $Z(r=0) \approx 0.69$, gradually decreasing to approximately $Z_s \approx 0.35$ at the boundary of the star. (b): This figure illustrates the mass (22) for the stellar SAX J1748.9-2021. The region denotes the observational limits on ($M = 1.85 \pm 0.25 M_\odot$ and $R = 12.35 \pm 0.11$ km) [85]. For $\zeta_1 = -0.05$, we employ the parameters of the model, i.e., [$C = 0.401$, $s_0 = 0.39$, $s_1 = -0.997$, $s_2 = 0.61$]. For $\zeta_1 = 0.05$, we use [$\zeta_1 = 0.05$, $C = 0.514$, $s_0 = 0.44$, $s_1 = -1.05$, $s_2 = 0.61$]. For $\zeta_1 = 0$ GR, we use [$s_0 = 0.42$, $s_1 = -1.03$, $s_2 = 0.61$].

- When $\zeta_1 = -0.05$, $M = 1.58 M_\odot$ for $R = 12.45$ km and $C = 0.401$. This determines the constant parameters to be [$\zeta_1 = -0.05$, $C = 0.401$, $s_0 = 0.39$, $s_1 = -0.997$, $s_2 = 0.61$].
- For $\zeta_1 = 0.05$, $M \approx 2.07 M_\odot$ for $R = 11.21$ km and $C = 0.514$. This determines the constant parameters ro be [$\zeta_1 = 0.05$, $C = 0.514$, $s_0 = 0.44$, $s_1 = -1.05$, $s_2 = 0.0.61$].
- For $\zeta_1 = 0$, the constant parameters are [$s_0 = 0.42$, $s_1 = -1.03$, $s_2 = 0.61$].

This imposes limits on $0 \leq |\zeta| \leq 5$ km^2. Generally, as represented in Fig. 2(b), the inclusion of $f(\mathcal{R})$ gravity results in variations in the stellar mass. In the analysis that follows, we'll utilize the specified numerical values to evaluate how robust current stellar is under different stability conditions.

D. The Zeldovich condition

An important criterion to confirm the pulsar's stability is provided by the study of Zeldovich [86]. According to this criterion, $p_r(r \to 0)$ will never be higher than the core energy density, which means that,

$$\frac{p_r(0)}{c^2 \rho(0)} \leq 1 \,. \tag{23}$$

Referring back to Eqs. (4) as detailed in the Supplementary Material, we can derive $\rho(r \to 0)$ and $p_r(r \to 0)$ as:

$$c^2 \rho(r \to 0) = -\frac{3 e^{-6\zeta_1(s_0 - s_2)} \left(156 {\zeta_1}^2 s_0 {s_2}^2 - s_2 - 2\zeta_1 {s_0}^2 - 120 {\zeta_1}^2 {s_0}^2 s_2 - 60 {\zeta_1}^2 {s_2}^3 + 24 {\zeta_1}^2 {s_0}^3 + 26 \zeta_1 s_2 s_0 - 20 \zeta_1 {s_2}^2\right)}{R^2 c^2 \kappa^2} \,,$$
$$p_r(r \to 0) = p_t(r \to 0)$$
$$= \frac{\left(e^{\zeta_1 s_2}\right)^6 \left(2 s_0 - s_2 - 240 {\zeta_1}^2 {s_0}^2 s_2 + 312 {\zeta_1}^2 s_0 {s_2}^2 + 46 \zeta_1 s_2 s_0 - 28 \zeta_1 {s_2}^2 - 10 \zeta_1 {s_0}^2 + 48 {\zeta_1}^2 {s_0}^3 - 120 {\zeta_1}^2 {s_2}^3\right)}{R^2 \kappa^2 \left(e^{\zeta_1 s_0}\right)^6} \,. \tag{24}$$

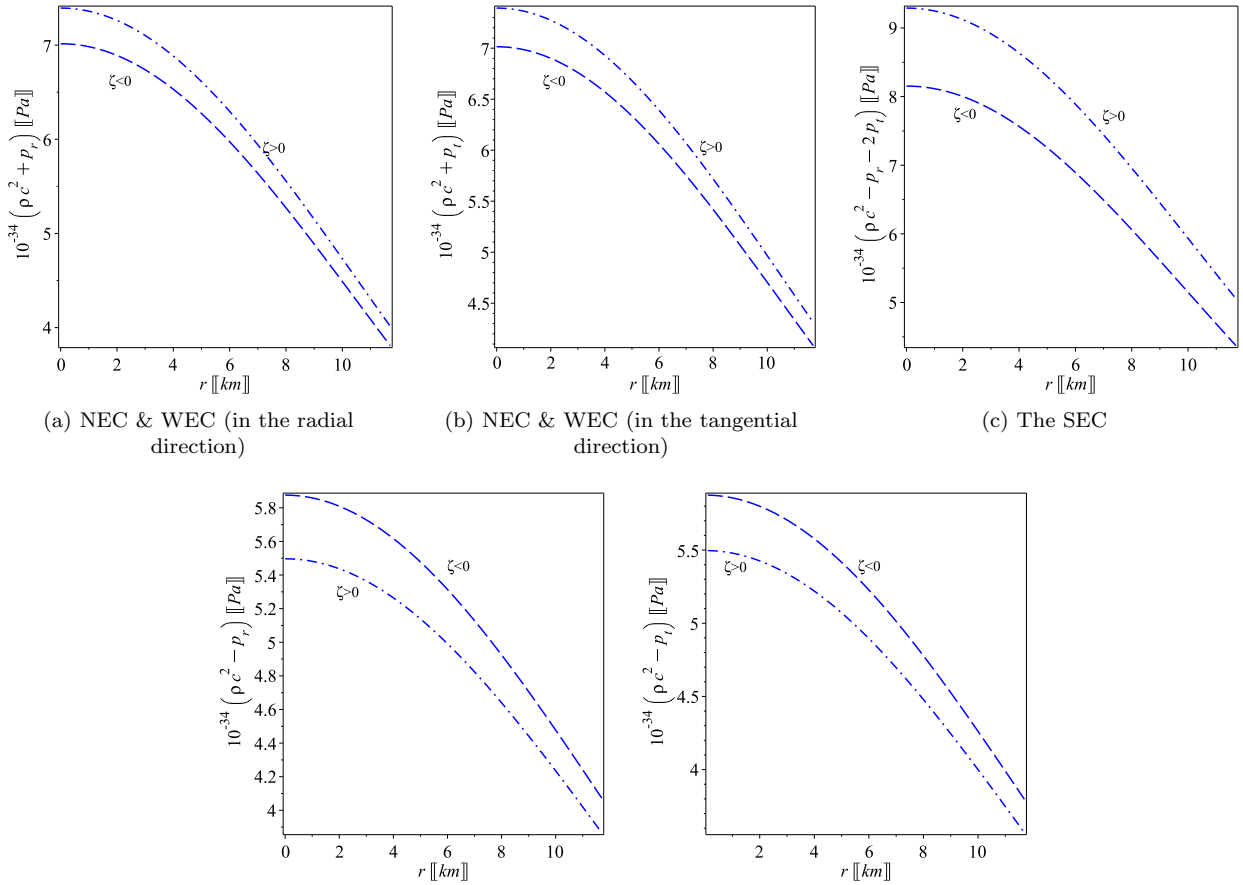

(a) NEC & WEC (in the radial direction)

(b) NEC & WEC (in the tangential direction)

(c) The SEC

(d) The DEC (in the radial direction)

(e) The DEC (in the tangential direction)

Figure 3. The reported graphs show that the effective matter $\bar{\mathbb{T}}_{\mu\nu}$ satisfies all the energy conditions, as elaborated in Subsection IV E, for the pulsar model SAX J1748.9-2021. The cases where $\zeta > 0$ and $\zeta < 0$ correspond to $\zeta_1 = 0.05$ and $\zeta_1 = -0.05$, respectively.

Utilizing the previous numerical values for the pulsar SAX J1748.9-2021, as discussed in Subsection IV C, we can assess the Zeldovich inequality (23). For $\zeta_1 = 0.05$, the inequality becomes $\frac{p_r(0)}{c^2\rho(0)} = 0.136$, which is less than 1. Similarly, for $\zeta_1 = -0.05$, the inequality reads $\frac{p_r(0)}{c^2\rho(0)} = 0.133$, also less than 1. This ensures the validation of the condition of Zeldovich.

E. The conditions of energy

It is advantageous to express Eqs. (2) as:

$$G_{\mu\nu} = \kappa \left(\mathbb{T}_{\mu\nu} + \mathbb{T}^{geom}_{\mu\nu}\right) = \kappa \bar{\mathbb{T}}_{\mu\nu} \,. \tag{25}$$

In this context, we use the notation $G_{\mu\nu} := \mathcal{R}_{\mu\nu} - g_{\mu\nu}\mathcal{R}/2$ to represent the Einstein tensor, which accounts for the correction arising from $f(\mathcal{R})$ gravity [19, 20] as:

$$T^{geom}_{\mu\nu} = \frac{1}{\kappa}\left(g_{\mu\nu}(f-\mathcal{R})/2 + \nabla_\mu\nabla_\nu f_{\mathcal{R}} - g_{\mu\nu}\Box f_{\mathcal{R}} + (1-f_{\mathcal{R}})\mathcal{R}_{\mu\nu}\right) \,. \tag{26}$$

The energy-momentum tensor can be written as $\bar{\mathbb{T}}_\mu{}^\nu = diag(-\bar{\rho}c^2, \bar{p}_r, \bar{p}_t, \bar{p}_t)$.

The focusing theorem and the Raychaudhuri equation imply the following inequalities for the tidal tensor: $R_{ab}u^a u^b \geq 0$ and $R_{ab}n^a n^b \geq 0$, where n^μ signifies an arbitrary future-directed null vector and u^μ represents an arbitrary timelike vector. It is worth noticing that, within $f(\mathcal{R})$ theory, the $\mathcal{R}$ could be expressed as $\mathcal{R}_{\mu\nu} =$

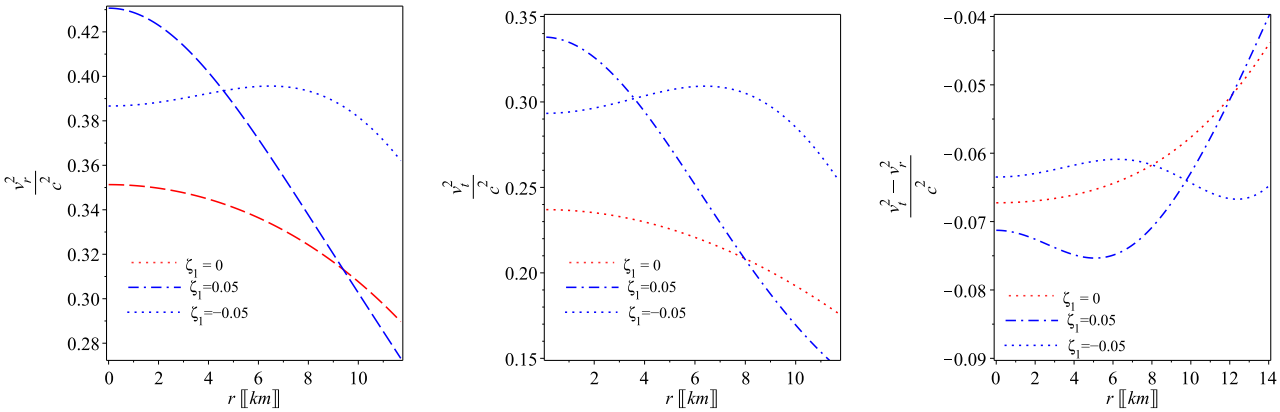

(a) $v_r{}^2$ (b) $v_t{}^2$ (c) Stability in the presence of strong anisotropy

Figure 4. The sound speed of stellar SAX J1748.9-2021 for $\zeta_1 = 0$, ± 0.05 is illustrated in the following way: (a) and (b) describe $v_r{}^2$ and $v_t{}^2$, respectively, as defined by (27). (c) demonstrates that the model adheres to the stability requirement $(v_t^2 - v_r^2)/c^2 < 0$ for the strong anisotropic case.

$\kappa\left(\bar{\mathbb{T}}_{\mu\nu} - \frac{1}{2}g_{\mu\nu}\bar{\mathbb{T}}\right)$, as can be inferred from Eq. (25). With this consideration in mind, the energy conditions (ECs) can be extended to $f(R)$ gravity in the following way [87]:

1. $\bar{\rho}c^2 + \bar{p}_r > 0$, $\bar{\rho}c^2 + \bar{p}_t > 0$, and $\bar{\rho} \geq 0$, which corresponds to the Weak Energy Condition (WEC).
2. $\bar{\rho}c^2 + \bar{p}_t \geq 0$, and $\bar{\rho}c^2 + \bar{p}_r \geq 0$, which corresponds to the Null Energy Condition (NEC).
3. $\bar{\rho}c^2 + \bar{p}_r \geq 0$, $\bar{\rho}c^2 + \bar{p}_t \geq 0$, $\bar{\rho}c^2 + \bar{p}_r + 2\bar{p}_t \geq 0$, which corresponds to the Strong Energy Condition (SEC).
4. $\bar{\rho}c^2 - |\bar{p}_r| \geq 0$, $\bar{\rho}c^2 - |\bar{p}_t| \geq 0$, $\bar{\rho} \geq 0$, which corresponds to the Dominant Energy Conditions (DEC).

Figure 3 provides a visual representation of the ECs when $\zeta_1 \gtrless 0$. These figures confirm that the current model of pulsar SAX J1748.9-2021 verifies all the conditions listed above.

F. Causality conditions

The condition of causality is consider as one of the fundamental aspects which states that the sound speed should not exceed the light speed. Referring to Eqs. (20), p_r and p_t can be fixed as:

$$v_r^2 = \frac{dp_r}{d\rho} = \frac{p_r'}{\rho'}, \quad v_t^2 = \frac{dp_t}{d\rho} = \frac{p_t'}{\rho'}\,. \tag{27}$$

Utilizing Eqs. (4) in the Supplementary Material, we can determine the gradients of density and pressure components, as provided by Eqs. (7) in the Supplementary Material. We represent v_r and v_t of pulsar SAX J1748.9-2021 when $\zeta_1 \gtrless 0$, as in Figs. 4(a) and (b). These figures show $0 \leq v_r^2/c^2 \leq 1$ and $0 \leq v_t^2/c^2 \leq 1$, satisfying the causality and stability conditions. Moreover, Fig. 4(c), illustrates that $-1 < (v_t^2 - v_r^2)/c^2 < 0$ throughout the interior of pulsar SAX J1748.9-2021 [88].

It is important to notice that the sound speed exhibits variations with r, as reported in Figs. 4(a) and (b). Specifically, when $\zeta_1 = 0.05$, we observe $0.27 < v_r^2/c^2 < 0.44$ and $0.15 < v_t^2/c^2 < 0.34$. Conversely, for $\zeta_1 = -0.05$, the intervals are $0.36 < v_r^2/c^2 < 0.39$ and $0.25 < v_t^2/c^2 < 0.30$. The maximum limits correspond to speed sound at $r = 0$, align perfectly the values derived in IV A from the induced EoSs (20), specifically $(\zeta_1 = 0.05, v_r^2 \approx 0.43c^2, v_t^2 \approx 0.337c^2)$ and $(\zeta_1 = -0.05, v_r^2 \approx 0.385c^2, v_t^2 \approx 0.29c^2)$.

G. The adiabatic and the equilibrium of hydrodynamic forces

In Newtonian gravity, it's widely accepted that there is no maximum limit on the mass of a stable configuration when the adiabatic index for a specific EoS increases 4/3. Conversely, within Newtonian gravity, it is necessary for a

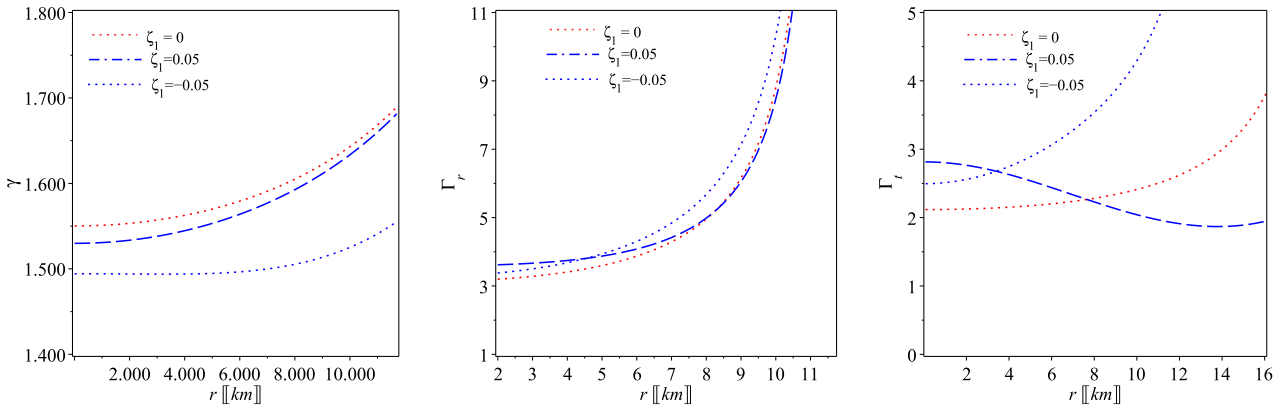

(a) Γ (b) Γ_r (c) Γ_t

Figure 5. The indices of adiabatic, provided by (28), for SAX J1748.9-2021. These figures ensure that throughout the interior of the pulsar that γ exceeds 4/3 and both Γ_r and Γ_t surpass γ.

stable configuration that $\gamma < 4/3$. Nevertheless, it has been shown that a star can withstand radial perturbations in a fully relativistic anisotropic neutron star model, even when $\gamma > 4/3$. To account for this, we define the adiabatic index [89, 90] as follows:

$$\gamma = \frac{4}{3}\left(1+\frac{\sigma}{r|p_r'|}\right)_{max}, \qquad \Gamma_r = \frac{\rho c^2 + p_r}{p_r} v_r^2, \qquad \Gamma_t = \frac{\rho c^2 + p_t}{p_t} v_t^2. \tag{28}$$

Obviously, in the case of isotropy ($\sigma = 0$), we obtain $\gamma = 4/3$. In the mildly anisotropic case ($\sigma < 0$), which is similar to the Newtonian theory, we have $\gamma < 4/3$, consistent with the standard stability requirement. On the other hand, when strong anisotropy is involved ($\sigma > 0$), similar to what is considered in this study, we find $\gamma > 4/3$ [90, 91].

By utilizing the field equations and Eqs. (4), and the gradients given by Eq. (7) presented in the Supplementary Material, we demonstrate that our $f(R)$ gravity offers a stable anisotropic model for the pulsar SAX J1748.9-2021 when $\zeta_1 \gtrless 0$, as illustrated in Figure 5."

Next, we examine the hydrodynamic equilibrium of the current model using the Tolman-Oppenheimer-Volkoff (TOV) equation, which is defined as follows:

$$F_a + F_g + F_h + F_{\mathcal{R}} = 0\,. \tag{29}$$

Here F_g, F_h, and F_a represent the typical gravitational, hydrostatic, and anisotropic forces, respectively, in additional to the force of F_R originating from the $f(R)$ component. These forces defined as:

$$\begin{aligned} \mathrm{F}_a &= \tfrac{2\Delta}{r}, \qquad F_g = -\tfrac{M_g}{r}(\rho c^2 + p_r)e^{\varepsilon/2}, \\ F_h &= \quad -p_t', \qquad F_{\mathcal{R}} = \zeta_1(c^2\rho' - p_r' - 2p_t')\,. \end{aligned} \tag{30}$$

Within the formula for the gravitational force, denoted as F_g, we have introduced the quantity $\varepsilon := \mu - \nu$, in addition to M_g which denotes the gravitational mass of a system that is isolated within the 3-space volume V (at constant time t). This can be described by the Tolman mass formula within the framework of $f(\mathcal{R})$ gravity. gravity, as described by Tolman in his 1930 work [92].

$$\begin{aligned} M_g(r) &= \int_V \left(\bar{\mathfrak{T}}^r{}_r + \bar{\mathfrak{T}}^\theta{}_\theta + \bar{\mathfrak{T}}^\phi{}_\phi - \bar{\mathfrak{T}}^t{}_t\right)\sqrt{-g}\,dV \\ &= e^{-\mu}(e^{\mu/2})' e^{\nu/2} r = \frac{1}{2} r\mu' e^{-\varepsilon/2}\,. \end{aligned} \tag{31}$$

Consequently, the gravitational force can be expressed as $\mathbb{F}_g = -\frac{s_0 r}{R^2}(\rho c^2 + p_r)$. Utilizing the field equations (4) together with the gradients (7) in the Supplementary Material, we can demonstrate that $f(\mathcal{R})$ gravity complies with (29), giving a stable model for the pulsar SAX J1748.9-2021 when $\zeta_1 \gtrless 0$, including ($\zeta_1 = 0$), as shown in Fig. 6.

Note that ($\sigma > 0$) introduces positive extra force which counters the field of gravity. This is an important to enlarge the star's size. As evident Figs. 6(b) and 6(c) demonstrate such phenomena with the additional force creating from $f(\mathcal{R})$ theory when $\zeta \gtrless 0$. This investigation aligns with the previously obtained results for the star SAX J1748.9-2021 in Subsection IV C, which yielded ($\zeta_1 = 0.05, M = 2.070 M_\odot, R = 11.21$ km$, C = 0.514$) and ($\zeta_1 = -0.05, M = 1.58 M_\odot, R = 12.45$ km$, C = 0.401$).

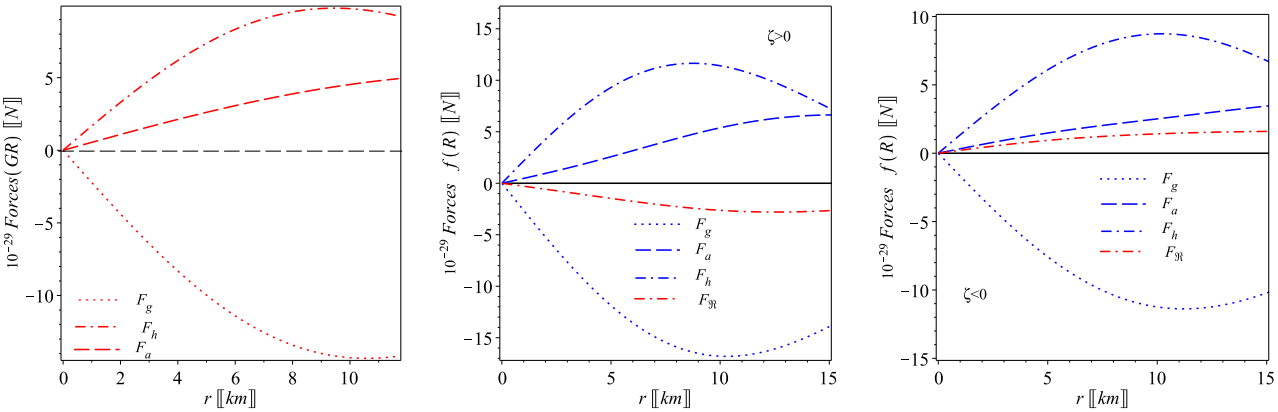

(a) The TOV of the GR case ($\zeta = 0$) (b) The TOV of $f(\mathcal{R})$: $\zeta > 0$ (c) The TOV of $f(\mathcal{R})$: $\zeta < 0$

Figure 6. The Tolman-Oppenheimer-Volkoff constraint, as described in Eq.(29), imposes various forces within the pulsar SAX J1748.9-2021. These forces are represented for $\zeta_1 = 0, \pm 0.05$. In the case of $\zeta_1 = 0.05$, the $f(\mathcal{R})$ the gravitational collapse force is further enhanced by correction, which adds an additional negative force. Conversely, for $\zeta_1 = -0.05$, $f(\mathcal{R})$ theory provides an extra positive force that lessens the force of gravitational collapse.

V. MASS-RADIUS RELATION AND EQUATION OF STATE

It is worth noticing that our study refrains from imposing specific EoS assumptions; rather, we use the ansatz of KB as outlined in Eqs. (15). Nevertheless, the resulting EoSs in Eqs.(20) show how pressures and density are related in this ansatz, and they are mainly valid at the core because of the power series assumptions that underlie it. By creating a range of density and pressure values that span from the core to the surface and take taking into account the model parameter's $\zeta_1 \gtrless 0$, we confirm the accuracy of these equations. ζ_1. We construct these sequences, as shown in Fig.7., using the numerical values given in Section IV C for the pulsar *SAX J1748.9-2021* and the equation of motions of $f(\mathcal{R})$ theory of gravity, which are specifically described in Eqs. (4), given in the Supplementary Material.

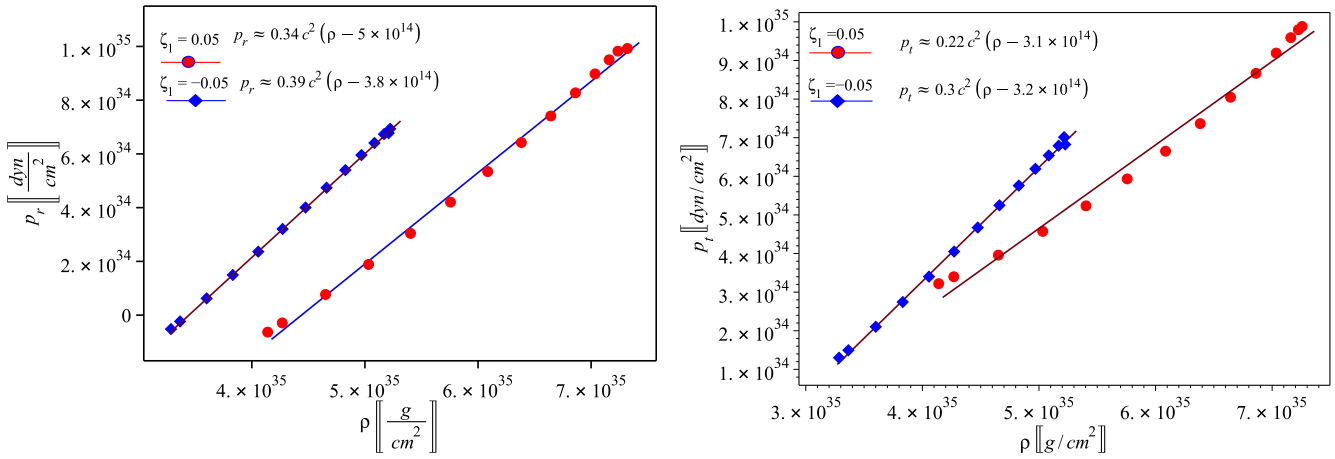

(a) EoS in the radial direction (b) EoSin the tangential direction

Figure 7. The optimal-fitting EoSs for the pulsar *SAX J1748.9-2021* are reported as follows: (a): We create a set of points for ρ and p_r using Eqs. (4), presented in the Supplementary Material for $\zeta = \pm 0.05$, where such points exhibit good alignment with a linear equation of state (EoS) pattern (b): Similarly, the data points also demonstrate a significant correlation with a linear model when tangential equations of state (EoS) with $\zeta = \pm 0.05$ are used. The correctness of these relations throughout the star's interior is confirmed by the linear EOSs best-fit, which agree with the equations derived before, specifically (20). It is worth noticing that, for the case $\zeta_1 = 0.05$, a slight deviation from the linear pattern can be observed, suggesting that $f(\mathcal{R})$ might present good fit, i.e., $p_{(rad.,tang.)}(\rho) \approx \tilde{a}_0 + \tilde{a}_1\rho + \tilde{a}_2\rho^2$ in this particular instance.

It is noteworthy that the linear best fit, in the both cases of positive/negative of ζ_1, induces slight alterations in the surface density and sound speeds. Consequently, we suggest that a higher polynomial, namely

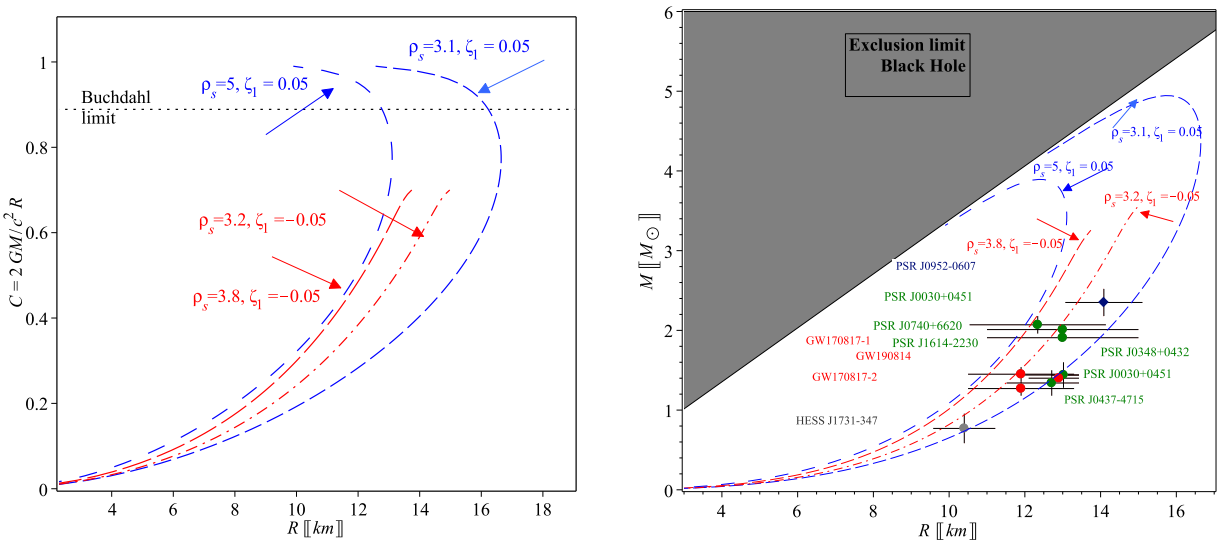

(a) C (b) MR

Figure 8. (a) Compactness-radius (CR) chart: The compactness of the Buchdahl limit is represented by the dotted horizontal line, where ($C = 8/9$). We graph the CR according to (EoSs) that fit best as outlined in Fig. 7. Additionally, we represent CR relation for distinct surface densities, specifically $\rho_I = 3.1 \times 10^{14}$ g/cm^3, $\rho_I = 3.2 \times 10^{14}$ g/cm^3, $\rho_I = 5 \times 10^{14}$ g/cm^3, and $\rho_I = 3.8 \times 10^{14}$ g/cm^3. It is worth noticing that, for $\zeta_1 = 0.05$, C can exceed the Buchdahl upper bound, a feature that is similar to the GR mode [77]. Interestingly, for $\zeta_1 = -0.05$, the higher value of C falls below the Buchdahl maximum limit, setting the difference between $f(\mathcal{R})$ gravity model and GR in such a study. (b) MR chart: When $\zeta \gtrless 0$, the MR curves cannot extend into non-physical branches.

$p_{r,t}(\rho) \approx \tilde{c}_0 + \tilde{c}_1\rho + \tilde{c}_2\rho^2$, could offer a more accurate fit, yielding non-linear equations of state.

As stated in [93], Buchdahl constructed a critical constraint on stable stellar configurations that places an upper limit on the C, i.e., $C < 8/9$. Notably, such boundary was initially developed for spherically symmetric isotropic (or slightly anisotropic) solutions inside GR.However, subsequent investigations have revealed that such constraints could be violated by an abundance of at least a single or many of these presumptions. With regard to stronger anisotropic models that are more realistic, the compactness can approach the limit of black hole, i.e., $C \to 1$, also within the framework of GR, as demonstrated in [94]. intriguingly, other limits impose more strict limits on C in cases featuring strong anisotropy, as indicated in [77, 95–97]. A similar conclusion has been reached when exploring scenarios involving nonminimal coupling between matter and geometry [98].

Within this context, it is worthwhile to look into this constraint in the context of $f(\mathcal{R})$ of gravity, as this study does. For generalized $f(\mathcal{R})$ theory of gravity, the Buchdahl limit is expressed as detailed in [99].

$$C = \frac{2GM}{c^2R} < \frac{4\frac{f_{\mathcal{R}}(r=R)}{f_{\mathcal{R}}(r=0)}\left[1+\frac{f_{\mathcal{R}}(r=R)}{f_{\mathcal{R}}(r=0)}\right]}{\left[1+2\frac{f_{\mathcal{R}}(r=R)}{f_{\mathcal{R}}(r=0)}\right]^2}.$$

In this study where, $f(\mathcal{R}) = \mathcal{R}e^{\zeta\mathcal{R}}$, for the compactness, we express the modified Buchdahl upper limit as

$$C < \frac{4(1+\zeta\mathcal{R}|_{r=R})e^{\zeta\mathcal{R}|_{r=R}}\left[(1+\zeta\mathcal{R}|_{r0})e^{\zeta R|_{r=0}} + (1+\zeta\mathcal{R}|_{r=R})e^{\zeta\mathcal{R}|_{r=R}}\right]}{\left[(1+\zeta\mathcal{R}|_{r0})e^{\zeta R|_{r=0}} + 2(1+\zeta\mathcal{R}|_{r=R})e^{\zeta\mathcal{R}|_{r=R}}\right]^2}. \tag{32}$$

We repeat that $\zeta = \zeta_1 R^2$ where R being the radius of the NS 11.7 km. Clearly Eq.(32) reduces to Buchdahl's GR if $\zeta = 0$ [93].

The Buchdahl limit for the pulsar SAX J1748.9-2021 can be computed as follows: We find $C \lesssim 0.891$ for $\zeta_1 = 0.05$, and $C \lesssim 0.895$ for $\zeta_1 = -0.05$, which different from GR.

We provide the corresponding MR relation in Fig. 8(b) when $\zeta_1 \gtrless 0$,where the matching condition (17) determines M; that is, $M = \frac{c^2R}{2G}(1 - e^{-s_2})$. This refers to the optimal EoS that was previously derived in this section. Consequently, we use $\zeta_1 = 0.05$ and the boundary density $\rho_I = 5 \times 10^{14}$ g/cm^3. This results in a maximal mass $M \approx 3.93M_\odot$ with $R \approx 12.7$ km. With $\zeta_1 = -0.05$ and a boundary density of $\rho_I = 3.8 \times 10^{14}$ g/cm^3, the maximum

mass $M = 3.275M_\odot$ is obtained at a radius of $R = 13.7$ km. Furthermore, we employ alternative boundary density values that yield a better fit with other pulsars while remaining consistent with the pulsar SAX J1748.9-2021, as shown in Fig. 8(b). Based on $\zeta_1 = 0.05$ and the boundary density $\rho_I = 3.1 \times 10^{14}$ g/cm^3, the maximum mass $M = 5.01M_\odot$ is found at radius $R = 16.05$ km. With $\zeta_1 = -0.05$ and $\rho_I = 3.2 \times 10^{14}$ g/cm^3, the maximum mass at radius $R = 15.02$ km is $M = 3.565M_\odot$. The MR curves clearly do not extend to the limit of black hole for positive ζ_1 cases, as depicted by the grey region in Fig. 8(b).

VI. DISCUSSION AND CONCLUSIONS

Several captivating and noteworthy discoveries emerge as soon as we delve into the realm of NSs within the framework of $f(\mathcal{R})$ theory of gravity. In our exploration, we placed our primary emphasis on the particular $f(\mathcal{R})$ model put forth as $f(\mathcal{R}) = \mathcal{R}e^{\zeta\mathcal{R}}$, and scrutinized its ramifications on the structural integrity and stability characteristics of neutron stars. To summarize our results:

- We investigated how $f(\mathcal{R})$ gravity (with $f(\mathcal{R}) \neq \mathcal{R}$) models alters the conventional understanding of neutron stars as described by GR. Examining the $f(\mathcal{R}) = \mathcal{R}e^{\zeta\mathcal{R}}$ function, we discovered that such adjustments can wield a substantial influence on the composition and dynamics of neutron stars. Our examination delved with the more practical setting of an anisotropic fluid behavior, assuming that the KB ansatz is followed by the inner region of the spherically symmetric stellar model. Concretely, we employed precise measurements derived from the radius and mass of star SAX J1748.9-2021, which boasts a mass of $2.07 \pm 0.11M_\odot$ and a radius within the range of $12.34^{+1.89}_{-1.67}$ km. These measurements served as valuable constraints on the parameter space of our current model, specifically influencing the value of ζ.

- One of our central concerns revolved around assessing the stability of neutron star configurations within the context of $f(\mathcal{R})$ gravity. We conducted an exhaustive analysis of various stability criteria, including the Zeldovich condition, energy conditions, and the speed of sound. Our results showed that $f(\mathcal{R})$ theory of gravity can verify these stipulations for certain parameter ranges. As we investigated, the allowable zone of $f(\mathcal{R})$ theory parameter, ζ is given by $|\zeta_1| < 0.05$. Different criteria of stability applied to our model from the viewpoint of geometry and matter confirmed its validity. Regarding the central density of pulsar SAX J1748.9-2021, our predictions are: When $\zeta_1 = 0.05$, $\rho_{\rm core} \approx 7.58 \times 10^{14}$ g/cm^3, that is 2.8 times the nuclear density ($\rho_{\rm nuc}$). Conversely, for $\zeta_1 = -0.05$, $\rho_{\rm core} \approx 6.78 \times 10^{14}$ g/cm^3, that is 2.5 times the nuclear density.

- In the frame of $f(\mathcal{R})$ theory, we derived the MR curve for NSs. Our results confirmed that NS mass and radius might be differ from the predictions of GR relying on how the form of $f(\mathcal{R})$. Such differences have critical consequences on the astrophysical observations and could be employ to calculate the validity of $\mathcal{R}e^{\zeta\mathcal{R}}$. More specific, we calculate the maximal mass $M = 4.0M_\odot$ corresponding to a radius of $R = 12.6$ km when $\zeta_1 = 0.05$ and a surface density of $\rho_I = 4.4 \times 10^{14}$ g/cm^3. On the other hand, we derive the maximal mass of $M = 4.1M_\odot$ with a corresponding radius $R = 14.4$ km when $\zeta_1 = -0.05$ and a surface density $\rho_I = 4.0 \times 10^{14}$ g/cm^3. Such findings are consistent with the properties of pulsar SAX J1748.9-2021 [100].

- We discussed the anisotropic properties and causality criteria of NSs in the frame of $f(\mathcal{R})$. Our discoveries revealed that, even in the presence of $f(\mathcal{R})$ modifications, the speed of sound remains consistent with causality constraints. We observed that the combined effects of strong anisotropy and $f(\mathcal{R})$ gravity, particularly when ζ is negative, act to counteract gravitational collapse and successfully lower the pulsar fluid's sound speed. Such results of maximal v_r, is $v_r^2 \approx 0.35c^2$, at the center of the neutron star. This finding aligns more closely with the soft EoSs predicted by gravitational wave observations, indicating a better agreement with astrophysical reality.

- In this study we show that the effect of anisotropy and within KB ansatz the pulsar could have exceed mass than that of GR. This case is similar to the isotropic case presented in [101] where the authors show that the maximum baryonic mass can exceed gravitational mass for for static NSs in the frame of $f(\mathcal{R})$.

In conclusion, our investigation implies that $f(\mathcal{R})$ gravity offers a fresh and captivating perspective for comprehending neutron stars. Although this realm of study continues to evolve, our results suggest that the $f(\mathcal{R})$ gravity frameworks can align with both theoretical stability criteria and empirical observations. The future exploration of this domain holds the promise of fine-tuning and scrutinizing these models more rigorously, potentially unveiling new revelations about the fundamental characteristics of gravity and the dynamics of compact objects such as neutron stars.

ACKNOWLEDGEMENTS

SC acknowledges the Istituto Nazionale di Fisica Nucleare (INFN) Sez. di Napoli, Iniziative Specifiche QGSKY and MOONLIGHT2 for the support. This paper is based upon work from COST Action CA21136 *Addressing observational tensions in cosmology with systematics and fundamental physics* (CosmoVerse) supported by COST (European Cooperation in Science and Technology).

[1] C. M. Will, Living reviews in relativity **17**, 1 (2014).
[2] B. P. Abbott et al., Physical review letters **121**, 129902 (2018).
[3] B. P. Abbott, R. Abbott, T. Abbott, F. Acernese, K. Ackley, C. Adams, T. Adams, P. Addesso, R. X. Adhikari, V. B. Adya, et al., Physical review letters **123**, 011102 (2019).
[4] A. A. Starobinsky, Physics Letters B **91**, 99 (1980).
[5] S. Capozziello, International Journal of Modern Physics D **11**, 483 (2002).
[6] S. M. Carroll, V. Duvvuri, M. Trodden, and M. S. Turner, Phys. Rev. D **70**, 043528 (2004), astro-ph/0306438.
[7] W. Hu and I. Sawicki, Phys. Rev. D **76**, 064004 (2007), 0705.1158.
[8] S. Nojiri and S. D. Odintsov, eConf **C0602061**, 06 (2006), hep-th/0601213.
[9] L. Amendola, R. Gannouji, D. Polarski, and S. Tsujikawa, Phys. Rev. D **75**, 083504 (2007), gr-qc/0612180.
[10] S. A. Appleby and R. A. Battye, Phys. Lett. B **654**, 7 (2007), 0705.3199.
[11] S. D. Odintsov and V. K. Oikonomou, Phys. Rev. D **101**, 044009 (2020), 2001.06830.
[12] K. Koyama, Rept. Prog. Phys. **79**, 046902 (2016), 1504.04623.
[13] S. Nojiri and S. D. Odintsov, Phys. Rev. D **68**, 123512 (2003), hep-th/0307288.
[14] S. Nojiri and S. D. Odintsov, Phys. Rev. D **77**, 026007 (2008), 0710.1738.
[15] G. Cognola, E. Elizalde, S. Nojiri, S. D. Odintsov, L. Sebastiani, and S. Zerbini, Phys. Rev. D **77**, 046009 (2008), 0712.4017.
[16] V. K. Oikonomou, Phys. Rev. D **103**, 044036 (2021), 2012.00586.
[17] V. K. Oikonomou, Phys. Rev. D **103**, 124028 (2021), 2012.01312.
[18] T. P. Sotiriou and V. Faraoni, Reviews of Modern Physics **82**, 451 (2010).
[19] A. De Felice and S. Tsujikawa, Living Reviews in Relativity **13**, 1 (2010).
[20] S. Capozziello and M. De Laurentis, Phys. Rept. **509**, 167 (2011), 1108.6266.
[21] S. Nojiri and S. D. Odintsov, Phys. Rept. **505**, 59 (2011), 1011.0544.
[22] T. Clifton, P. G. Ferreira, A. Padilla, and C. Skordis, Physics reports **513**, 1 (2012).
[23] S. Nojiri, S. Odintsov, and V. Oikonomou, Physics Reports **692**, 1 (2017).
[24] S. S. Yazadjiev, D. D. Doneva, K. D. Kokkotas, and K. V. Staykov, JCAP **06**, 003 (2014), 1402.4469.
[25] A. V. Astashenok, S. Capozziello, and S. D. Odintsov, Phys. Lett. B **742**, 160 (2015), 1412.5453.
[26] S. S. Yazadjiev and D. D. Doneva (2015), 1512.05711.
[27] F. Sbisà, P. O. Baqui, T. Miranda, S. E. Jorás, and O. F. Piattella, Phys. Dark Univ. **27**, 100411 (2020), 1907.08714.
[28] A. V. Astashenok, S. Capozziello, S. D. Odintsov, and V. K. Oikonomou, Phys. Lett. B **811**, 135910 (2020), 2008.10884.
[29] A. V. Astashenok, S. Capozziello, S. D. Odintsov, and V. K. Oikonomou, Phys. Lett. B **816**, 136222 (2021), 2103.04144.
[30] A. V. Astashenok, S. Capozziello, S. D. Odintsov, and V. K. Oikonomou, EPL **134**, 59001 (2021), 2106.01234.
[31] K. Nobleson, A. Ali, and S. Banik, Eur. Phys. J. C **82**, 32 (2022).
[32] J. C. Jiménez, J. M. Z. Pretel, E. S. Fraga, S. E. Jorás, and R. R. R. Reis, JCAP **07**, 017 (2022), 2112.09950.
[33] R. Abbott, T. Abbott, S. Abraham, F. Acernese, K. Ackley, C. Adams, R. X. Adhikari, V. Adya, C. Affeldt, M. Agathos, et al., The Astrophysical Journal Letters **896**, L44 (2020).
[34] G. G. L. Nashed and E. N. Saridakis, Phys. Rev. D **102**, 124072 (2020), 2010.10422.
[35] A. V. Astashenok and S. D. Odintsov, Mon. Not. Roy. Astron. Soc. **493**, 78 (2020), 2001.08504.
[36] A. V. Astashenok and S. D. Odintsov, Mon. Not. Roy. Astron. Soc. **498**, 3616 (2020), 2008.11271.
[37] G. J. Olmo, D. Rubiera-Garcia, and A. Wojnar, Physics Reports **876**, 1 (2020).
[38] C. G. Boehmer, T. Harko, and F. S. N. Lobo, Astropart. Phys. **29**, 386 (2008), 0709.0046.
[39] V. K. Sharma, B. K. Yadav, and M. M. Verma, Eur. Phys. J. C **81**, 109 (2021), 2011.02878.
[40] S. Capozziello, V. F. Cardone, and A. Troisi, Phys. Rev. D **73**, 104019 (2006), astro-ph/0604435.
[41] G. G. L. Nashed, Adv. High Energy Phys. **2018**, 7323574 (2018).
[42] S. Capozziello, V. F. Cardone, and A. Troisi, Mon. Not. Roy. Astron. Soc. **375**, 1423 (2007), astro-ph/0603522.
[43] C. F. Martins and P. Salucci, Mon. Not. Roy. Astron. Soc. **381**, 1103 (2007), astro-ph/0703243.
[44] G. G. L. Nashed and S. Nojiri, Phys. Rev. D **102**, 124022 (2020), 2012.05711.
[45] S. C. Jaryal and A. Chatterjee, Eur. Phys. J. C **81**, 273 (2021), 2102.08717.
[46] A. K. Sharma and M. M. Verma, Astrophys. J. **926**, 29 (2022).
[47] S. Capozziello, M. De Laurentis, R. Farinelli, and S. D. Odintsov, Phys. Rev. D **93**, 023501 (2016), 1509.04163.
[48] M. Chaichian, S. S. Masood, C. Montonen, A. Perez Martinez, and H. Perez Rojas, Phys. Rev. Lett. **84**, 5261 (2000), hep-ph/9911218.
[49] E. J. Ferrer, V. de la Incera, J. P. Keith, I. Portillo, and P. L. Springsteen, Phys. Rev. C **82**, 065802 (2010), 1009.3521.

[50] D. Horvat, S. Ilijic, and A. Marunovic, Class. Quant. Grav. **28**, 025009 (2011), 1010.0878.
[51] D. D. Doneva and S. S. Yazadjiev, Phys. Rev. D **85**, 124023 (2012), 1203.3963.
[52] H. O. Silva, C. F. Macedo, E. Berti, and L. C. Crispino, Classical and Quantum Gravity **32**, 145008 (2015).
[53] K. Yagi and N. Yunes, Phys. Rev. D **91**, 123008 (2015), 1503.02726.
[54] B. Ivanov, The European Physical Journal C **77**, 1 (2017).
[55] A. Isayev, Physical Review D **96**, 083007 (2017).
[56] B. Biswas and S. Bose, Physical Review D **99**, 104002 (2019).
[57] S. K. Maurya, A. Banerjee, M. K. Jasim, J. Kumar, A. K. Prasad, and A. Pradhan, Phys. Rev. D **99**, 044029 (2019), 1811.09890.
[58] J. M. Pretel, The European Physical Journal C **80**, 726 (2020).
[59] A. Rahmansyah, A. Sulaksono, A. B. Wahidin, and A. M. Setiawan, Eur. Phys. J. C **80**, 769 (2020).
[60] S. Das, S. Ray, M. Khlopov, K. Nandi, and B. K. Parida, Annals of Physics **433**, 168597 (2021).
[61] S. Das, K. N. Singh, L. Baskey, F. Rahaman, and A. K. Aria, General Relativity and Gravitation **53**, 1 (2021).
[62] D. Deb, B. Mukhopadhyay, and F. Weber, Astrophys. J. **922**, 149 (2021), 2108.12436.
[63] A. Rahmansyah and A. Sulaksono, Phys. Rev. C **104**, 065805 (2021).
[64] G. H. Bordbar and M. Karami, The European Physical Journal C **82**, 74 (2022).
[65] V. Folomeev, Physical Review D **97**, 124009 (2018).
[66] G. Panotopoulos, T. Tangphati, A. Banerjee, and M. K. Jasim, Phys. Lett. B **817**, 136330 (2021), 2104.00590.
[67] G. Nashed, S. D. Odintsov, and V. Oikonomou, The European Physical Journal C **81**, 528 (2021).
[68] M. F. Shamir and A. Malik, Chin. J. Phys. **69**, 312 (2021).
[69] A. Malik, A. Ashraf, U. Naqvi, and Z. Zhang, Int. J. Geom. Meth. Mod. Phys. **19**, 2250073 (2022).
[70] M. Farasat Shamir and A. Malik, Commun. Theor. Phys. **71**, 599 (2019).
[71] G. G. L. Nashed and W. El Hanafy (2023), 2306.13396.
[72] A. Malik, New Astron. **93**, 101765 (2022).
[73] A. Malik, I. Ahmad, and Kiran, Int. J. Geom. Meth. Mod. Phys. **19**, 2250028 (2022).
[74] A. Usman and M. F. Shamir, New Astron. **91**, 101691 (2022).
[75] M. Ahmad, G. Mustafa, and M. F. Shamir, Int. J. Mod. Phys. A **36**, 2150203 (2021).
[76] G. G. Nashed and S. Capozziello, The European Physical Journal C **80**, 1 (2020).
[77] Z. Roupas and G. G. Nashed, The European Physical Journal C **80**, 1 (2020).
[78] K. D. Krori and J. Barua, Journal of Physics A **8**, 508 (1975).
[79] F. Özel, T. Güver, and D. Psaltis, The Astrophysical Journal **693**, 1775 (2009).
[80] S. S. Yazadjiev and D. D. Doneva (2015), 1512.05711.
[81] H. A. Buchdahl, Physical Review **116**, 1027 (1959).
[82] B. V. Ivanov, Physical Review D **65**, 104011 (2002).
[83] D. E. Barraco, V. H. Hamity, and R. J. Gleiser, Physical Review D **67**, 064003 (2003).
[84] C. Böhmer and T. Harko, Classical and Quantum Gravity **23**, 6479 (2006).
[85] I. Legred, K. Chatziioannou, R. Essick, S. Han, and P. Landry, Phys. Rev. D **104**, 063003 (2021), 2106.05313.
[86] Y. B. Zeldovich and I. D. Novikov, Relativistic astrophysics. Vol. 1: Stars and relativity, Chicago: University of Chicago Press (1971).
[87] S. Capozziello, F. S. N. Lobo, and J. P. Mimoso, Phys. Rev. D **91**, 124019 (2015), 1407.7293.
[88] L. Herrera, Phys. Lett. A **165**, 206 (1992).
[89] S. Chandrasekhar, Astrophys. J. **140**, 417 (1964), [Erratum: Astrophys.J. 140, 1342 (1964)].
[90] R. Chan, L. Herrera, and N. Santos, Monthly Notices of the Royal Astronomical Society **265**, 533 (1993).
[91] H. Heintzmann and W. Hillebrandt, Astronomy and Astrophysics **38**, 51 (1975).
[92] R. C. Tolman, Physical Review **35**, 896 (1930).
[93] H. A. Buchdahl, Phys. Rev. **116**, 1027 (1959), URL https://link.aps.org/doi/10.1103/PhysRev.116.1027.
[94] A. Alho, J. Natário, P. Pani, and G. Raposo, Phys. Rev. D **106**, L041502 (2022), 2202.00043.
[95] A. Alho, J. Natário, P. Pani, and G. Raposo, Phys. Rev. D **105**, 044025 (2022), [Erratum: Phys.Rev.D 105, 129903 (2022)], 2107.12272.
[96] G. Raposo, P. Pani, M. Bezares, C. Palenzuela, and V. Cardoso, Phys. Rev. D **99**, 104072 (2019), 1811.07917.
[97] V. Cardoso and P. Pani, Living Rev. Rel. **22**, 4 (2019), 1904.05363.
[98] G. Nashed and W. E. Hanafy, The European Physical Journal C **82**, 679 (2022).
[99] R. Goswami, S. D. Maharaj, and A. M. Nzioki, Phys. Rev. D **92**, 064002 (2015), 1506.04043.
[100] G. G. L. Nashed, Astrophys. J. **950**, 129 (2023), 2306.10273.
[101] A. V. Astashenok, S. Capozziello, S. D. Odintsov, and V. K. Oikonomou, EPL **136**, 59001 (2021), 2111.14179.

Constraining $f(\mathcal{R})$ gravity by Pulsar SAX J1748.9-2021 observations: Supplementary material

Gamal G. L. Nashed*
Centre for Theoretical Physics, The British University, P.O. Box 43, El Sherouk City, Cairo 11837, Egypt.

Salvatore Capozziello†
Dipartimento di Fisica E. Pancini, Universit'a di Napoli Federico II Complesso Universitario di Monte Sant Angelo, Edificio G, Via Cinthia, I-80126, Napoli, Italy, Scuola Superiore Meridionale, Largo S. Marcellino 10, I-80138, Napoli, Italy, and Istituto Nazionale di Fisica Nucleare (INFN), Sez. di Napoli Complesso Universitario di Monte Sant Angelo, Edificio G, Via Cinthia, I-80126, Napoli, Italy.

(Dated: May 17, 2024)

We report here, for the interested reader, the various components of the energy-momentum tensor and the form of them after substituting the KB ansatz. Moreover, we report the gradient components of the energy-momentum tensor.

arXiv:2405.09590v1 [gr-qc] 15 May 2024

* nashed@bue.edu.eg
† capozziello@na.infn.it

I. THE COMPONENTS OF THE ENERGY MOMENTUM TENSOR

The components of the energy-momentum tensor are given as:

$$\rho \equiv \frac{1}{r^8 c^2 \kappa} e^{\frac{1}{2r^2}\left\{-\zeta\left(2\mu'' r^2+\mu'^2 r^2+\left(-\nu' r^2+4r\right)\mu'-4\nu' r+4\right)e^{-\nu}+4\zeta-8\nu r^2\right\}}\Bigg\{-\zeta\Bigg[\zeta r^2 e^{\nu}\mu''-2\left(\zeta+r^2\right)e^{2\nu}+\frac{\zeta}{2}\Bigg(\mu'^2 r^2+\left(4r-\nu' r^2\right)\mu''$$

$$+4-4\nu' r\Bigg)e^{\nu}\Bigg]r^6\mu''''+\left(\zeta r^2\mu''+\frac{1}{2}\zeta\mu'^2 r^2-\frac{1}{2}r\zeta\left(\nu' r-4\right)\mu'-2\zeta\nu' r-\left(2\zeta+3r^2\right)e^{\nu}+2\zeta\right)\zeta^2 r^6\mu'''^2+2\Bigg[\Bigg(2-\frac{3}{2}\nu' r$$

$$+\mu' r\Bigg)\zeta^2 r^4\mu''^2-\frac{\zeta r^3\mu''}{2}\Bigg[r\zeta\left(\mu' r+4\right)\nu''-\zeta r^2\mu'^3+\left(\frac{7}{2}\zeta r^2\nu'-6\zeta r\right)\mu'^2+\left(-\frac{5}{2}\zeta r^2\nu'^2+16\zeta\nu' r+\left(4\zeta+7r^2\right)e^{\nu}-8\zeta\right)\mu'$$

$$-10\zeta r\nu'^2+\left(14\zeta-6\left(\zeta+2r^2\right)e^{\nu}\right)\nu'+16re^{\nu}\Bigg]-\frac{1}{4}\left(\mu' r+4\right)\zeta\left(\zeta\mu'^2 r^2-r\zeta\left(\nu' r-4\right)\mu'-4\zeta\nu' r-\left(4\zeta+6r^2\right)e^{\nu}+4\zeta\right)r^2\nu''$$

$$+\left(r^3\left(r^2+\zeta\right)\mu'+\left(-3r^5-3\zeta r^3\right)\nu'+4r^4-8\zeta r^2-8\zeta^2\right)e^{2\nu}-\frac{1}{4}\Bigg[\zeta\mu'^4 r^5\nu'+\left(8\zeta r^4\nu'-2\zeta r^5\nu'^2+r^3\left(e^{\nu}r^2+4\zeta\right)\right)\left(\mu'\right)^3$$

$$+\Bigg(\zeta\nu'^3 r^3-16\zeta r^2\nu'^2-10r\left(\left(r^2+\frac{2}{5}\zeta\right)e^{\nu}-\frac{8}{5}\zeta\right)\nu'+8\left(r^2-\zeta\right)e^{\nu}+24\zeta\Bigg)r^2\mu'^2+9\Bigg[\frac{8}{9}\zeta\nu'^3 r^3+\left(\left(r^2+\frac{4}{9}\zeta\right)e^{\nu}-4\zeta\right)r^2$$

$$\left(\nu'\right)^2-\frac{44}{9}\left(\left(2/11\zeta+r^2\right)e^{\nu}+2/11\zeta\right)r\nu'-\left(\frac{16}{3}\zeta+\frac{4}{9}r^2\right)e^{\nu}+\frac{16}{3}\zeta\Bigg]r\mu'+16\zeta\left(\nu'\right)^3 r^3+36\left(\left(r^2+\frac{4}{9}\zeta\right)e^{\nu}-\frac{4}{9}\zeta\right)r^2\nu'^2$$

$$-28r\left(\left(-\frac{8}{7}\zeta+r^2\right)e^{\nu}+\frac{8}{7}\zeta\right)\nu'+\left(-32r^2-64\zeta\right)e^{\nu}+32\zeta\Bigg]\zeta\Bigg]\zeta r^3\mu'''+\frac{1}{2}\left(\mu' r+4\right)\zeta r^5\nu'''\Bigg[\zeta r^2 e^{\nu}\mu''-2\left(\zeta+r^2\right)e^{2\nu}$$

$$+\frac{1}{2}\zeta\left(\mu'^2 r^2+\left(-\left(\nu'\right)r^2+4r\right)\mu'+4-4\left(\nu'\right)r\right)e^{\nu}\Bigg]+\left(\zeta\mu'^2 r^2+\left(4\zeta r-3\zeta r^2\nu'\right)\mu'+\frac{9}{4}\zeta r^2\nu'^2+4\zeta-e^{\nu}r^2-6\zeta\nu' r\right)\zeta^2 r^6\mu''^3$$

$$-\Bigg[\left(\zeta\mu'^2 r^2-\frac{3}{2}r\zeta\left(\nu' r-4\right)\mu'-6\zeta\left(\nu'\right)r-2e^{\nu}r^2+8\zeta\right)\zeta r^2\nu''-\left(2\zeta r^2-\frac{3}{2}r^4\right)e^{2\nu}-\frac{1}{2}\zeta\Bigg[\zeta\mu'^4 r^4+\left(8\zeta r^3-6\zeta r^4\nu'\right)\mu'^3$$

$$+\left(\frac{41}{4}\zeta r^4\nu'^2-38\zeta\nu' r^3-7\left(\left(r^2+\frac{4}{7}\zeta\right)e^{\nu}-\frac{16}{7}\zeta\right)r^2\right)\mu'^2-\frac{21}{4}\Bigg[\zeta\nu'^3 r^2-\frac{68}{7}\zeta r\nu'^2+\left(\left(-\frac{16}{7}\zeta-\frac{32}{7}r^2\right)e^{\nu}+\frac{80}{7}\zeta\right)\nu'$$

$$+\frac{128}{21}re^{\nu}\Bigg]r^2\mu'-21\zeta\nu'^3 r^3+\left(\left(-9\zeta r^2-19r^4\right)e^{\nu}+49\zeta r^2\right)\nu'^2+\left(-16\zeta r+56r^3e^{\nu}\right)\nu'+\left(16\zeta-28r^2\right)e^{\nu}-16\zeta\Bigg]\Bigg]\zeta r^4\mu''^2$$

$$+\frac{1}{4}\Bigg[r^4\zeta^2\left(\mu' r+4\right)^2\nu''^2-2\Bigg[8\left(\zeta r+r^3\right)e^{2\nu}+\left(\zeta r^3\mu'^4+\left(10\zeta r^2-\frac{7}{2}\zeta\nu' r^3\right)\mu'^3+\frac{5\mu'^2 r}{2}\Bigg[\zeta r^2\nu'^2-12\zeta\nu' r+\frac{64}{5}\zeta-e^{\nu}\Bigg(\frac{18}{5}r^2$$

$$+\frac{8}{5}\zeta\Bigg)\Bigg]+\left(20\zeta r^2\nu'^2+\left(\left(6\zeta r+\frac{29}{2}r^3\right)e^{\nu}-78\zeta r\right)\nu'-\left(16\zeta+50r^2\right)e^{\nu}+32\zeta\right)\mu'+40\zeta r\nu'^2+\Bigg[\left(58r^2+24\zeta\right)e^{\nu}-56\zeta\Bigg]\nu'$$

$$-60re^{\nu}\Bigg)\zeta\Bigg]r^3\nu''+\Bigg[-2\mu'^2 r^6+\left(\left(-18r^6-20\zeta r^4\right)\nu'-64r\zeta^2+8r^5-80\zeta r^3\right)\mu'+\left(22\zeta r^4+22r^6\right)\nu'^2+\Bigg[96r\zeta^2-60r^5$$

$$+88\zeta r^3\Bigg]\nu'-64\zeta^2-176\zeta r^2-4r^4\Bigg]e^{2\nu}+4r^4e^{3\nu}-2\zeta\Bigg\{\zeta r^6\nu'\mu'^5-4\zeta\left(-1+r^2\left(\nu'\right)^2-\frac{5}{2}\nu' r\right)r^4\mu'^4+5\Bigg[\zeta\nu'^3 r^3-\frac{36}{5}\zeta r^2\nu'^2$$

$$-\frac{17}{10}r\left(\left(\frac{8}{17}\zeta+r^2\right)e^{\nu}-\frac{44}{17}\zeta\right)\nu'+\left(\frac{2}{5}r^2-\frac{8}{5}\zeta\right)e^{\nu}+\frac{32}{5}\zeta\Bigg]r^3\mu'^3-2\Bigg[\zeta r^4\nu'^4-21\zeta\nu'^3 r^3+\Bigg[48\zeta r^2-\left(5\zeta r^2+\frac{87}{8}r^4\right)e^{\nu}\Bigg]\nu'^2$$

$$+\left(\left(29r^3-2\zeta r\right)e^{\nu}+18\zeta r\right)\nu'+\left(32\zeta+8r^2\right)e^{\nu}-44\zeta\Bigg]r^2\left(\mu'\right)^2-\frac{53}{4}r\Bigg[\frac{64}{53}\zeta r^4\nu'^4+\left(\left(\frac{24}{53}\zeta+r^2\right)e^{\nu}-\frac{408}{53}\zeta\right)r^3\nu'^3$$

$$-\frac{436}{53}\left(\left(\frac{28}{109}\zeta+r^2\right)e^{\nu}-\frac{52}{109}\zeta\right)r^2\nu'^2+\frac{240}{53}\left(\left(-2\zeta+r^2\right)e^{\nu}+\frac{38}{15}\zeta\right)r\nu'+\left(\frac{352}{53}r^2+\frac{512}{53}\zeta\right)e^{\nu}-\frac{384}{53}\zeta\Bigg]\mu'-32\zeta r^4\nu'^4$$

$$+\left(56\zeta r^3-\left(24\zeta r^3+53r^5\right)e^{\nu}\right)\nu'^3+\left(\left(95r^4-48\zeta r^2\right)e^{\nu}+48\zeta r^2\right)\nu'^2+52\left(\left(\frac{40}{13}\zeta+r^2\right)e^{\nu}-\frac{28}{13}\zeta\right)r\nu'-\left(88r^2+64\zeta\right)e^{\nu}$$

$$+32\zeta\Bigg\}\Bigg]\zeta r^2\mu''+\frac{1}{8}\left(\mu' r+4\right)^2\zeta^2\left(\zeta\mu'^2 r^2-r\zeta\left(\nu' r-4\right)\mu'-4\zeta\nu' r-\left(4\zeta+6r^2\right)e^{\nu}+4\zeta\right)r^4\nu''^2+\frac{1}{4}\Bigg[\Bigg(\left(-4\zeta r^4-4r^6\right)\mu'^2$$

$$+\left(\left(14\zeta r^4+14r^6\right)\nu'+32r\zeta^2-24r^5+24\zeta r^3\right)\mu'+\left(56r^5+56\zeta r^3\right)\nu'+176\zeta r^2-16r^4+128\zeta^2\Bigg)e^{2\nu}+\zeta\Bigg(\zeta r^6\nu'\mu'^5$$

$$-2\left(-6\zeta\nu' r-\frac{1}{2}e^{\nu}r^2-2\zeta+\zeta r^2\nu'^2\right)r^4\mu'^4+\Bigg[\zeta\nu'^3 r^3-24\zeta r^2\nu'^2-2\frac{1}{2}r\left(\left(\frac{8}{21}\zeta+r^2\right)e^{\nu}-\frac{32}{7}\zeta\right)\nu'+\left(-8\zeta+10r^2\right)e^{\nu}$$

$$
\begin{aligned}
&+ 40\zeta\Big] r^3\mu'^3 + 19/2\Big(\frac{24}{19}\zeta\nu'^3 r^3 + r^2\left(\left(r^2+\frac{8}{19}\zeta\right)e^{\nu} - \frac{200}{19}\zeta\right)\nu'^2 - \frac{172}{19}\left(\left(r^2+\frac{12}{43}\zeta\right)e^{\nu} - \frac{28}{43}\zeta\right)r\nu' + \Big(\frac{16}{19}r^2 \\
&- \frac{160}{19}\zeta\Big)e^{\nu} + \frac{288}{19}\zeta\Big)r^2\mu'^2 + 76\Big[\frac{12}{19}\zeta\nu'^3 r^3 + \left(\left(r^2+\frac{8}{19}\zeta\right)e^{\nu} - \frac{40}{19}\zeta\right)r^2\nu'^2 - \frac{97}{38}\left(e^{\nu}r^2 + \frac{32}{97}\zeta\right)r\nu' - \Big[\frac{26}{19}r^2 + \frac{64}{19}\zeta\Big] \\
&e^{\nu} + \frac{56}{19}\zeta\Big]r\mu' + 64\zeta\left(\nu'\right)^3 r^3 + 152\left(\left(r^2+\frac{8}{19}\zeta\right)e^{\nu} - \frac{8}{19}\zeta\right)r^2\left(\nu'\right)^2 - 72\Big[\left(-\frac{16}{9}\zeta + r^2\right)e^{\nu} + \frac{16}{9}\zeta\Big]r\nu' \\
&+ \left(-176r^2 - 256\zeta\right)e^{\nu} + 128\zeta\Big)\Big]\zeta r^2\nu'' - \frac{1}{8}\Big[\mu'^4 r^8 + \left(8r^7 - 2r^8\nu'\right)\mu'^3 + \Big[\left(-12r^6\zeta - 11r^8\right)\nu'^2 + \left(4r^7 - 64\zeta^2 r^3 - 88r^5\zeta\right)\nu' \\
&- 16\zeta r^4 - 64\zeta^2 r^2 + 20r^6\Big]\mu'^2 + 12\Big[r^5\left(r^2+\zeta\right)\nu'^3 + \left(10/3\zeta r^4 + 16/3\zeta^2 r^2 - 5r^6\right)\nu'^2 + \left(-3r^5 - \frac{104}{3}\zeta r^3 - 16r\zeta^2\right)\nu' \\
&- \frac{128}{3}\zeta^2 + 4/3r^4 - \frac{112}{3}\zeta r^2\Big]r\mu' + \left(48r^7 + 48r^5\zeta\right)\nu'^3 + \left(-32r^6 + 256\zeta^2 r^2 + 384\zeta r^4\right)\nu'^2 + \left(-96r^5 - 64\zeta r^3 + 256r\zeta^2\right)\nu' \\
&- 64r^4 - 896\zeta r^2 - 768\zeta^2\Big]\zeta e^{2\nu} + \Big(\frac{1}{2}\zeta\mu'^2 r^6 - \frac{1}{2}r^5\zeta\left(\nu' r - 4\right)\mu' + r^3\left(r^4 - 4\zeta r^2 - 4\zeta^2\right)\nu' - 56\zeta^2 r^2 - 8\zeta r^4 - r^6 - 32\zeta^3\Big)e^{3\nu} \\
&+ e^{4\nu}r^6 + 1/8\zeta^2\Big[\zeta\nu'^2\mu'^6 r^8 - 3\zeta\nu' r^6\left(-\frac{8}{3} - 4\nu' r + r^2\nu'^2\right)\left(\mu'\right)^5 + 3\Big[\zeta r^4\nu'^4 - 12\zeta\nu'^3 r^3 - 3\Big[\left(r^2+\frac{4}{9}\zeta\right)e^{\nu} - 4\zeta\Big]r^2\nu'^2 \\
&+ 4/3\left(\left(r^2 - 4\zeta\right)e^{\nu} + 20\zeta\right)r\nu' + \frac{16}{3}\zeta\Big]r^4\mu'^4 - r^3\Big[\zeta\nu'^5 r^5 - 36\zeta r^4\nu'^4 - 18\left(\left(r^2+\frac{4}{9}\zeta\right)e^{\nu} - 8\zeta\right)r^3\nu'^3 + \left(80r^4 e^{\nu} + 64\zeta r^2\right)\nu'^2 \\
&+ 36r\left(\left(\frac{40}{9}\zeta + r^2\right)e^{\nu} - \frac{68}{9}\zeta\right)\nu' + 64\zeta\left(e^{\nu} - 2\right)\Big]\mu'^3 - 9\Big[\frac{4}{3}\zeta\nu'^5 r^5 + \left(\left(r^2+\frac{4}{9}\zeta\right)e^{\nu} - \frac{148}{9}\zeta\right)r^4\nu'^4 - \frac{148}{9}\Big[\left(\frac{12}{37}\zeta + r^2\right)e^{\nu} \\
&- \frac{44}{37}\zeta\Big]r^3\nu'^3 + 16\left(\left(r^2 - \frac{14}{9}\zeta\right)e^{\nu} + \frac{10}{3}\zeta\right)r^2\nu'^2 + \frac{104}{3}\left(\left(r^2+\frac{56}{39}\zeta\right)e^{\nu} - \frac{40}{39}\zeta\right)r\nu' + \left(\frac{448}{9}\zeta + \frac{112}{9}r^2\right)e^{\nu} - \frac{128}{3}\zeta\Big]r^2\mu'^2 \\
&- 72\Big[\frac{2}{3}\zeta\nu'^5 r^5 + \left(\left(r^2 + 4/9\zeta\right)e^{\nu} - \frac{28}{9}\zeta\right)r^4\nu'^4 + \left(-9/2r^5 e^{\nu} - \frac{16}{9}\zeta r^3\right)\nu'^3 - \frac{29}{9}\left(\left(\frac{96}{29}\zeta + r^2\right)e^{\nu} - \frac{88}{29}\zeta\right)r^2\nu'^2 \\
&+ \frac{20}{3}\left(\left(\frac{4}{15}\zeta + r^2\right)e^{\nu} + 2/15\zeta\right)r\nu' + \left(\frac{56}{9}r^2 + \frac{128}{9}\zeta\right)e^{\nu} - \frac{64}{9}\zeta\Big]r\mu' - 64\zeta\nu'^5 r^5 - 144\left(\left(r^2 + 4/9\zeta\right)e^{\nu} - 4/9\zeta\right)r^4\nu'^4 \\
&+ 80\left(\left(r^2 - \frac{16}{5}\zeta\right)e^{\nu} + \frac{16}{5}\zeta\right)r^3\left(\nu'\right)^3 + 448\left(\left(r^2+\frac{8}{7}\zeta\right)e^{\nu} - 4/7\zeta\right)r^2\nu'^2 - 32r\left(\left(-16\zeta + r^2\right)e^{\nu} + 8\zeta\right)\nu' \\
&+ \left(-768\zeta - 448r^2\right)e^{\nu} + 256\zeta\Big]\Big\}, \qquad (1)
\end{aligned}
$$

$$
\begin{aligned}
p_r \equiv{}& \frac{-1}{8r^6\kappa} e^{\frac{-\left(2r^2\mu''+\mu'^2r^2+\left(4r-r^2\nu'\right)\mu'+4-4\nu'r\right)\zeta e^{-\nu}+4\zeta-6\nu r^2}{2r^2}} \Big\{ -2r^3\left(\mu' r+4\right)\zeta\Big[2\zeta r^2\mu''+\zeta\mu'^2r^2-r\zeta\left(-4+\left(\nu'\right)r\right)\mu'-4\zeta\nu' r+4\zeta \\
&-4\left(r^2+\zeta\right)e^{\nu}\Big]\mu'''-4r^4\zeta\left(\zeta\mu'^2r^2-3/2r\zeta\left(\nu' r-4\right)\mu'+e^{\nu}r^2-6\zeta\nu' r+8\zeta\right)\mu''^2-2r^3\zeta\Big[-\zeta r\left(\mu' r+4\right)^2\nu''-4re^{2\nu}+\zeta r^3\mu'^4 \\
&+\left(10\zeta r^2-7/2\nu' r^3\zeta\right)\mu'^3+5/2r\left(\zeta r^2\left(\nu'\right)^2-12\zeta\left(\nu'\right)r+\left(-4/5r^2-8/5\zeta\right)e^{\nu}+\frac{64}{5}\zeta\right)\mu'^2+\Big\{20\zeta r^2\nu'^2+4r\Big[\left(r^2+3/2\zeta\right)e^{\nu} \\
&-\frac{39}{2}\zeta\Big]\nu'+\left(-16\zeta-20r^2\right)e^{\nu}+32\zeta\Big\}\mu'+40\zeta r\left(\nu'\right)^2+\left(\left(16r^2+24\zeta\right)e^{\nu}-56\zeta\right)\nu'-28e^{\nu}r\Big]\mu''+r^2\left(\mu' r+4\right)^2\zeta \\
&\left(\zeta\mu'^2r^2-r\zeta\left(-4+\nu' r\right)\mu'-4\zeta\nu' r+\left(-4r^2-4\zeta\right)e^{\nu}+4\zeta\right)\nu''+\Big[4\zeta\mu'^2r^4+\left(32r^3\zeta+32r\zeta^2-4r^4\zeta\nu'-8r^5\right)\mu'-8r^4+128\zeta^2 \\
&-16\nu' r^3\zeta+128\zeta r^2\Big]e^{2\nu}+8e^{3\nu}r^4+\Big[\zeta\mu'^5\nu' r^6-2r^4\left(-6\zeta\left(\nu'\right)r-2\zeta+\zeta r^2\nu'^2+1/2e^{\nu}r^2\right)\mu'^4+r^3\Big(\zeta\nu'^3r^3-24\zeta r^2\nu'^2 \\
&-2r\left(\left(r^2+2\zeta\right)e^{\nu}-24\zeta\right)\nu'-4\left(2\zeta+r^2\right)e^{\nu}+40\zeta\Big)\mu'^3+3r^2\Big(4\zeta\nu'^3r^3+r^2\left(\left(4/3\zeta+r^2\right)e^{\nu}-\frac{100}{3}\zeta\right)\nu'^2 \\
&-\frac{20}{3}r\left(\left(\frac{6}{5}\zeta+r^2\right)e^{\nu}-\frac{14}{5}\zeta\right)\nu'+\left(-\frac{20}{3}r^2-\frac{80}{3}\zeta\right)e^{\nu}+48\zeta\Big)\mu'^2+24r\Big[2\zeta\nu'^3r^3+r^2\left(\left(4/3\zeta+r^2\right)e^{\nu}-\frac{20}{3}\zeta\right)\nu'^2-\Big(\frac{8}{3}r\zeta \\
&+\frac{11}{6}r^3e^{\nu}\Big)\nu'-\left(\frac{32}{3}\zeta+4r^2\right)e^{\nu}+\frac{28}{3}\zeta\Big]\mu'+64\zeta\nu'^3r^3+48r^2\left(\left(\frac{4}{3}\zeta+r^2\right)e^{\nu}-\frac{4}{3}\zeta\right)\nu'^2+16r\left(\left(8\zeta+r^2\right)e^{\nu}-8\zeta\right)\nu' \\
&-128\left(2\zeta+r^2\right)e^{\nu}+128\zeta\Big]\zeta\Big\}, \qquad (2)
\end{aligned}
$$

$$p_t \equiv -\frac{1}{8r^8\kappa}e^{\frac{-\left(2r^2\mu''+\mu'^2r^2+\left(-r^2\nu'+4r\right)\mu'+4-4\nu'r\right)\zeta e^{-\nu}+4\zeta-8\nu r^2}{2r^2}}\Big\{-4r^6\Big[2\zeta r^2e^{\nu}\mu''-4\left(r^2+\zeta\right)e^{2\nu}+e^{\nu}\zeta\Big(\mu'^2r^2+\left(4r-r^2\nu'\right)\mu'+4$$

$$-4\nu'r\Big)\Big]\zeta\mu''''+4r^6\zeta^2\left(2\zeta r^2\mu''+\zeta\mu'^2r^2-r\zeta\left(\nu'r-4\right)\mu'-4\zeta\nu'r-\left(6r^2+4\zeta\right)e^{\nu}+4\zeta\right)\mu'''^2-4r^3\Big[-4r^4\zeta^2\Big(2-\frac{3}{2}\nu'r$$

$$+\mu'r\Big)\mu''^2-2r^3\Big[-r\zeta\left(\left(\mu'\right)r+4\right)\nu''+\zeta r^2\mu'^3+\left(6r\zeta-\frac{7}{2}\zeta\nu'r^2\right)\mu'^2+\left(\frac{5}{2}\zeta r^2\nu'^2-16\zeta\nu'r-\left(4\zeta+\frac{15}{2}r^2\right)e^{\nu}+8\zeta\right)\mu'$$

$$+10\zeta r\nu'^2+\left(\left(12r^2+6\zeta\right)e^{\nu}-14\zeta\right)\nu'-15e^{\nu}r\Big]\zeta\mu'+r^2\left(\mu'r+4\right)\zeta\left(\zeta\mu'^2r^2-r\zeta\left(\nu'r-4\right)\mu'-4\zeta\nu'r-\left(6r^2+4\zeta\right)e^{\nu}+4\zeta\right)\nu''$$

$$+\left(\left(-6r^5-6r^3\zeta\right)\mu'+\left(12r^3\zeta+12r^5\right)\nu'-12r^4+32\zeta^2+36\zeta r^2\right)e^{2\nu}+\Big[\zeta\mu'^4r^5\nu'-2r^3\left(\zeta r^2\nu'^2-2\zeta-3/4e^{\nu}r^2-4\zeta\nu'r\right)\mu'^3$$

$$+r^2\Big(\zeta\nu'^3r^3-16\zeta r^2\nu'^2-\frac{21}{2}r\Big(\Big(\frac{8}{21}\zeta+r^2\Big)e^{\nu}-\frac{32}{21}\zeta\Big)\nu'+\left(9r^2-8\zeta\right)e^{\nu}+24\zeta\Big)\mu'^2+9r\Big(\frac{8}{9}\zeta\nu'^3r^3+r^2\Big[\Big(r^2+\frac{4}{9}\zeta\Big)e^{\nu}$$

$$-4\zeta\Big]\nu'^2-5r\Big(\Big(\frac{8}{45}\zeta+r^2\Big)e^{\nu}+\frac{8}{45}\zeta\Big)\nu'+\left(-16/3\zeta-2/3r^2\right)e^{\nu}+16/3\zeta\Big)\mu'+16\zeta\nu'^3r^3+36r^2\Big(\Big(r^2+\frac{4}{9}\zeta\Big)e^{\nu}-\frac{4}{9}\zeta\Big)\nu'^2$$

$$-24r\Big(\Big(r^2-\frac{4}{3}\zeta\Big)e^{\nu}+\frac{4}{3}\zeta\Big)\nu'-\left(64\zeta+36r^2\right)e^{\nu}+32\zeta\Big]\zeta\Big]\zeta\mu'''+2r^5\Big[2\zeta r^2e^{\nu}\mu''-4\left(r^2+\zeta\right)e^{2\nu}+e^{\nu}\zeta\Big\{\mu'^2r^2+4-4\nu'r$$

$$+\left(4r-r^2\nu'\right)\mu'\Big\}\Big]\left(\mu'r+4\right)\zeta\nu'''+8r^6\zeta^2\Big(\zeta\left(\mu'\right)^2r^2+\left(4r\zeta-3\zeta\nu'r^2\right)\mu'+\frac{9}{4}\zeta r^2\left(\nu'\right)^2+4\zeta-e^{\nu}r^2-6\zeta\nu'r\Big)\mu'^3$$

$$+4r^4\Big[-2r^2\Big(\zeta\left(\mu'\right)^2r^2-3/2r\zeta\left(-4+\nu'r\right)\mu'-2e^{\nu}r^2+8\zeta-6\zeta\nu'r\Big)\zeta\nu''+\left(4\zeta r^2+4r^4\right)e^{2\nu}+\Big[\zeta\mu'^4r^4+\left(8r^3\zeta-6r^4\zeta\nu'\right)\mu'^3$$

$$+\Big(\frac{41}{4}\zeta\nu'^2r^4-38\nu'r^3\zeta-8r^2\left(\left(r^2+1/2\zeta\right)e^{\nu}-2\zeta\right)\Big)\mu'^2-\frac{21}{4}r^2\Big(\zeta\nu'^3r^2-\frac{68}{7}\zeta r\nu'^2+\Big(\Big(-\frac{16}{7}\zeta-\frac{34}{7}r^2\Big)e^{\nu}+\frac{80}{7}\zeta\Big)\nu'$$

$$+\frac{128}{21}e^{\nu}r\Big)\mu'-21\zeta\left(\nu'\right)^3r^3+\left(\left(-19r^4-9\zeta r^2\right)e^{\nu}+49\zeta r^2\right)\nu'^2+\left(-16r\zeta+53r^3e^{\nu}\right)\nu'+\left(16\zeta-24r^2\right)e^{\nu}-16\zeta\Big]\zeta\Big]\zeta\mu''^2$$

$$-4r^2\Big\{-\frac{1}{2}\zeta^3r^4\left(\mu'r+4\right)^2\nu'^2+r^3\Big[\left(8r\zeta+8r^3\right)e^{2\nu}+\Big(\zeta r^3\left(\mu'\right)^4+\left(10\zeta r^2-7/2\nu'r^3\zeta\right)\mu'^3+5/2r\Big(\zeta r^2\nu'^2-12\zeta\nu'r$$

$$+\Big(-8/5\zeta-\frac{19}{5}r^2\Big)e^{\nu}+\frac{64}{5}\zeta\Big)\mu'^2+\Big(20\zeta r^2\nu'^2+\Big(\Big(\frac{29}{2}r^3+6r\zeta\Big)e^{\nu}-78r\zeta\Big)\nu'+\left(-51r^2-16\zeta\right)e^{\nu}+32\zeta\Big)\mu'+40\zeta r\nu'^2$$

$$+\left(\left(24\zeta+58r^2\right)e^{\nu}-56\zeta\right)\nu'-56e^{\nu}r\Big)\zeta\Big]\zeta\nu''-2\Big[r^4\left(r^2+\zeta\right)\mu'^2+\left(-13/2r^4\left(r^2+\zeta\right)\nu'+7/2r^5-16r\zeta^2-22r^3\zeta\right)\mu'$$

$$+11/2r^4\left(r^2+\zeta\right)\nu'^2+\Big(25r^3\zeta-\frac{25}{2}r^5+24r\zeta^2\Big)\nu'-16\zeta^2-44\zeta r^2-5r^4\Big]\zeta e^{2\nu}+r^4\left(r^2-2\zeta\right)e^{3\nu}+\Big[\zeta\left(\mu'\right)^5\nu'r^6$$

$$-4r^4\Big(\zeta r^2\nu'^2-\frac{5}{2}\zeta\nu'r-\zeta-\frac{1}{8}e^{\nu}r^2\Big)\mu'^4+5r^3\mu'^3\Big(\zeta\nu'^3r^3-\frac{36}{5}\zeta r^2\nu'^2-\frac{41}{20}r\Big(\Big(r^2+\frac{16}{41}\zeta\Big)e^{\nu}-\frac{88}{41}\zeta\Big)\nu'+\Big(\frac{4}{5}r^2-\frac{8}{5}\zeta\Big)e^{\nu}$$

$$+\frac{32}{5}\zeta\Big)-2r^2\Big(\zeta\nu'^4r^4-21\zeta\nu'^3r^3+\Big(\Big(-5\zeta r^2-\frac{23}{2}r^4\Big)e^{\nu}+48\zeta r^2\Big)\nu'^2+\Big(\Big(\frac{125}{4}r^3-2r\zeta\Big)e^{\nu}+18r\zeta\Big)\nu'+\left(9r^2+32\zeta\right)e^{\nu}$$

$$-44\zeta\Big)\left(\mu'\right)^2-\frac{53}{4}r\Big(\frac{64}{53}\zeta\nu'^4r^4+r^3\Big(\Big(r^2+\frac{24}{53}\zeta\Big)e^{\nu}-\frac{408}{53}\zeta\Big)\left(\nu'\right)^3-\frac{446}{53}r^2\Big(\Big(\frac{56}{223}\zeta+r^2\Big)e^{\nu}-\frac{104}{223}\zeta\Big)\nu'^2$$

$$+\frac{204}{53}r\Big(\Big(r^2-\frac{40}{17}\zeta\Big)e^{\nu}+\frac{152}{51}\zeta\Big)\nu'+\Big(\frac{384}{53}r^2+\frac{512}{53}\zeta\Big)e^{\nu}-\frac{384}{53}\zeta\Big)\mu'-32\zeta\nu'^4r^4+\left(\left(-53r^5-24r^3\zeta\right)e^{\nu}+56r^3\zeta\right)\nu'^3$$

$$+\left(\left(85r^4-48\zeta r^2\right)e^{\nu}+48\zeta r^2\right)\nu'^2+66r\Big(\Big(\frac{80}{33}\zeta+r^2\Big)e^{\nu}-\frac{56}{33}\zeta\Big)\nu'+\left(-64\zeta-88r^2\right)e^{\nu}+32\zeta\Big]\zeta^2\Big\}\mu''+r^4\left(\mu'r+4\right)^2\zeta^2$$

$$\times\left(\zeta\mu'^2r^2-r\zeta\left(-4+\nu'r\right)\mu'-4\zeta\nu'r+\left(-6r^2-4\zeta\right)e^{\nu}+4\zeta\right)\nu''^2+2r^2\Big\{\Big[\left(-6r^6-6r^4\zeta\right)\mu'^2+\Big(\left(14r^6+14r^4\zeta\right)\nu'-28r^5$$

$$+20r^3\zeta+32r\zeta^2\Big)\mu'+\left(56r^5+56r^3\zeta\right)\nu'+128\zeta^2+192\zeta r^2\Big]e^{2\nu}+\Big[\zeta\mu'^5\nu'r^6-2r^4\left(-6\zeta\nu'r+\zeta r^2\nu'^2-2\zeta-3/4e^{\nu}r^2\right)\mu'^4$$

$$+r^3\left(\zeta\nu'^3r^3-24\zeta r^2\nu'^2+\left(48r\zeta-\left(11r^3+4r\zeta\right)e^{\nu}\right)\nu'+\left(13r^2-8\zeta\right)e^{\nu}+40\zeta\right)\mu'^3+\frac{19}{2}r^2\Big[\frac{24}{19}\zeta\nu'^3r^3+r^2\Big(\Big(\frac{8}{19}\zeta+r^2\Big)e^{\nu}$$

$$-\frac{200}{19}\zeta\Big)\nu'^2-\frac{178}{19}r\Big(\Big(\frac{24}{89}\zeta+r^2\Big)e^{\nu}-\frac{56}{89}\zeta\Big)\nu'+\Big(-\frac{160}{19}\zeta+\frac{20}{19}r^2\Big)e^{\nu}+\frac{288}{19}\zeta\Big]\mu'^2+76r\Big[\frac{12}{19}\zeta\nu'^3r^3+r^2\Big(\Big(\frac{8}{19}\zeta+r^2\Big)e^{\nu}$$

$$-\frac{40}{19}\zeta\Big)\nu'^2-\frac{97}{38}r\Big(e^{\nu}r^2+\frac{32}{97}\zeta\Big)\nu'+\Big(-\frac{29}{19}r^2-\frac{64}{19}\zeta\Big)e^{\nu}+\frac{56}{19}\zeta\Big]\mu'+64\zeta\nu'^3r^3+152r^2\Big(\Big(\frac{8}{19}\zeta+r^2\Big)e^{\nu}-\frac{8}{19}\zeta\Big)\nu'^2$$

$$
\begin{aligned}
&- 56r\left(\left(r^2-\frac{16}{7}\zeta\right)e^{\nu}+\frac{16}{7}\zeta\right)\nu'+\left(-192r^2-256\zeta\right)e^{\nu}+128\zeta\Big]\zeta\Big\}\zeta\nu''-4\zeta\Big[r^5\left(r\left(r^2+\zeta\right)\nu'+1/2r^2+2\zeta\right)\mu'^3-4r^2\\
&\left(r^4\left(r^2+\zeta\right)\nu'^2+\left(4r\zeta^2-\frac{5}{4}r^5+\frac{11}{2}r^3\zeta\right)\nu'-\frac{7}{4}r^4-\zeta r^2+4\zeta^2\right)\mu'^2+3r\Big(r^5\left(r^2+\zeta\right)\nu'^3+\left(\frac{16}{3}\zeta^2r^2+\frac{8}{3}r^4\zeta-\frac{35}{6}r^6\right)\nu'^2\\
&+\left(-16r\zeta^2-\frac{116}{3}r^3\zeta-\frac{17}{3}r^5\right)\nu'-40\zeta r^2-\frac{128}{3}\zeta^2+2r^4\Big)\mu'+\left(12r^7+12\zeta r^5\right)\nu'^3+\left(104r^4\zeta+2r^6+64\zeta^2r^2\right)\nu'^2\\
&+\left(-30r^5+64r\zeta^2\right)\nu'-192\zeta^2-256\zeta r^2-28r^4\Big]e^{2\nu}+\Big(\left(-2r^8+4r^6\zeta\right)\mu'^2+2r^3\left(r^3\left(r^2-2\zeta\right)\nu'+28\zeta r^2+16\zeta^2-2r^4\right)\mu'\\
&+\left(-56\zeta r^5-32\zeta^2r^3+4r^7\right)\nu'-256\zeta^3-512\zeta^2r^2-96r^4\zeta\Big)e^{3\nu}+\Big[-16r^4e^{4\nu}+\Big\{\zeta\nu'^2\mu'^6r^8-3r^6\nu'\Big(\zeta r^2\nu'^2-4\zeta\nu'r-\frac{8}{3}\zeta\\
&-1/3e^{\nu}r^2\Big)\mu'^5+3r^4\Big(\zeta\nu'^4r^4-12\zeta\nu'^3r^3-11/3r^2\left(\left(r^2+4/11\zeta\right)e^{\nu}-\frac{36}{11}\zeta\right)\nu'^2+10/3r\left(\left(-8/5\zeta+r^2\right)e^{\nu}+8\zeta\right)\nu'\\
&+4/3e^{\nu}r^2+16/3\zeta\Big)\mu'^4-r^3\Big[\zeta\nu'^5r^5-36\zeta\nu'^4r^4+\left(\left(-19r^5-8r^3\zeta\right)e^{\nu}+144r^3\zeta\right)\nu'^3+\left(64\zeta r^2+92r^4e^{\nu}\right)\nu'^2\\
&+36r\left(\left(\frac{40}{9}\zeta+r^2\right)e^{\nu}-\frac{68}{9}\zeta\right)\nu'+\left(64\zeta-16r^2\right)e^{\nu}-128\zeta\Big]\mu'^3-9r^2\Big[4/3\zeta\nu'^5r^5+r^4\left(\left(r^2+4/9\zeta\right)e^{\nu}-\frac{148}{9}\zeta\right)\nu'^4\\
&-\frac{154}{9}r^3\left(\left(r^2+\frac{24}{77}\zeta\right)e^{\nu}-\frac{8}{7}\zeta\right)\nu'^3+\frac{148}{9}r^2\left(\left(r^2-\frac{56}{37}\zeta\right)e^{\nu}+\frac{120}{37}\zeta\right)\nu'^2+\frac{352}{9}r\left(\left(r^2+\frac{14}{11}\zeta\right)e^{\nu}-\frac{10}{11}\zeta\right)\nu'\\
&+\left(\frac{448}{9}\zeta+\frac{112}{9}r^2\right)e^{\nu}-\frac{128}{3}\zeta\Big]\mu'^2-72r\Big[2/3\zeta\nu'^5r^5+r^4\left(\left(r^2+4/9\zeta\right)e^{\nu}-\frac{28}{9}\zeta\right)\nu'^4+\left(-9/2r^5e^{\nu}-\frac{16}{9}r^3\zeta\right)\nu'^3\\
&-4r^2\left(\left(r^2+8/3\zeta\right)e^{\nu}-\frac{22}{9}\zeta\right)\nu'^2+\frac{62}{9}r\left(\left(r^2+\frac{8}{31}\zeta\right)e^{\nu}+\frac{4}{31}\zeta\right)\nu'+\left(\frac{128}{9}\zeta+\frac{64}{9}r^2\right)e^{\nu}-\frac{64}{9}\zeta\Big]\mu'-64\zeta\nu'^5r^5\\
&-144\left(\left(r^2+4/9\zeta\right)e^{\nu}-4/9\zeta\right)r^4\nu'^4+48r^3\left(\left(-16/3\zeta+r^2\right)e^{\nu}+16/3\zeta\right)\nu'^3+480r^2\left(\left(\frac{16}{15}\zeta+r^2\right)e^{\nu}-\frac{8}{15}\zeta\right)\nu'^2\\
&+32r\left(\left(16\zeta+r^2\right)e^{\nu}-8\zeta\right)\nu'+\left(-512r^2-768\zeta\right)e^{\nu}+256\zeta\Big\}\zeta\Big]\zeta\Big\},
\end{aligned}
\tag{3}
$$

II. THE FORM OF THE COMPONENTS OF ρ, p_r AND p_t ADOPTING THE KB ANSATZ

$$
\begin{aligned}
\rho = {} & \frac{1}{c^2 r^8 R^{16}\kappa}\Bigg\{ -56R^4\Bigg[\frac{12}{7}\left(R^4 - r^2\left(s_0 - 2s_2\right)R^2 + r^4 s_0 s_2\right)\left(R^2 + r^2\left(s_0 - s_2\right)\right)\Bigg(R^6 + 2\left(s_0 - \frac{s_2}{2}\right)r^2 R^4 + \frac{r^4}{3}\left(2s_0 s_2 - 2{s_2}^2\right. \\
& \left. + {s_0}^2\right)R^2 + \frac{r^6 s_0 s_2}{3}\left(s_0 - s_2\right)\Bigg)\zeta + r^2\Bigg(R^{12} + \frac{3}{7}r^2\left(s_0 + 4s_2\right)R^{10} - \frac{8}{7}\left(\frac{13}{8}{s_2}^2 + {s_0}^2 - \frac{41}{8}s_0 s_2\right)r^4 R^8 + \frac{9}{7}r^6\Bigg({s_0}^3 - \frac{16}{3}{s_0}^2 s_2 \\
& + \frac{34}{3}s_0{s_2}^2 - \frac{16}{3}{s_2}^3\Bigg)R^6 + \frac{9}{7}r^8\left(\frac{223}{9}{s_0}^2{s_2}^2 + {s_0}^4 + 4{s_2}^4 - \frac{29}{3}{s_0}^3 s_2 - \frac{172}{9}{s_2}^3 s_0\right)R^4 - \frac{20}{7}s_0\left(s_0 - s_2\right)r^{10} s_2\Bigg(\frac{9}{5}{s_2}^2 - \frac{37}{10}s_0 s_2 \\
& + {s_0}^2\Bigg)R^2 + \frac{9r^{12}}{7}{s_0}^2{s_2}^2\left(s_0 - s_2\right)^2\Bigg)\Bigg]\zeta^2 X(r) + 32\left(R^4 - r^2\left(s_0 - 2s_2\right)R^2 + r^4 s_0 s_2\right)^2\left(R^2 + r^2\left(s_0 - s_2\right)\right)^2\Bigg(R^4 + 3\Bigg(s_0 r^2 R^2 \\
& - \frac{2s_2}{3}\Bigg) + r^4 s_0\left(s_0 - s_2\right)\Bigg)\zeta^3 X_1(r) + \Bigg(8\Bigg(12\left(R^6 + r^2 s_0 R^4 - 1/3r^4\left(-7s_0 s_2 + {s_0}^2 + 4{s_2}^2\right)R^2 + 2/3r^6 s_0 s_2\left(s_0 - s_2\right)\right)R^2\zeta^2 \\
& + 14r^2\zeta\Bigg(R^8 + 3/14r^2\left(s_0 + 13/3s_2\right)R^6 - 4/7\left(s_0 - 1/2s_2\right)\left(s_0 - \frac{17}{4}s_2\right)r^4 R^4 + \frac{5}{14}r^6 s_2\left(4/5s_0 s_2 + {s_0}^2 - 6/5{s_2}^2\right)R^2 \\
& + \frac{3}{14}r^8 s_0{s_2}^2\left(s_0 - s_2\right)\Bigg) + \Bigg(R^8 - 3/4\left(s_0 - 8/3s_2\right)r^2 R^6 + 1/2\left({s_0}^2 - \frac{41}{2}s_0 s_2 + 18{s_2}^2\right)r^4 R^4 - 3/2r^6\left(4{s_0}^2 s_2 - 11s_0{s_2}^2\right. \\
& \left. + 4{s_2}^3 + {s_0}^3\right)R^2 - 1/4r^8 s_0\left(s_0 - s_2\right)\left(s_0 + 3s_2\right)\left(-4s_2 + s_0\right)\Bigg)r^4\Bigg)\zeta X_2(r) + \Bigg(\Bigg(-32R^4\zeta^3 + \left(-8s_2 r^4 R^2 - 56R^4 r^2\right)\zeta^2 \\
& - 8\left(R^2 - r^2\left(s_0 - s_2\right)\right)r^4\left(1/4r^2 s_0 + R^2\right)\zeta + 2R^2 s_2 r^8 - R^4 r^6\Bigg)X_3(r) + R^4 X_4(r) r^6\Bigg)R^4\Bigg)R^8\Bigg\}, \\
p_r = {} & \frac{1}{r^6 R^{12}\kappa}\Bigg\{16R^4\zeta\Bigg(\left(r^2 + 2\zeta\right)R^8 + 5/8\left(\left(6/5s_2 + s_0\right)r^2 + \frac{32}{5}\left(s_0 - 1/4s_2\right)\zeta\right)r^2 R^6 - \frac{1}{2}r^4\Bigg(\Bigg(3{s_2}^2 + {s_0}^2 - \frac{27}{4}s_0 s_2\Bigg)r^2 \\
& - 3\left(5/3s_0 s_2 + {s_0}^2 - 4/3{s_2}^2\right)\zeta\Bigg)R^4 + 2\left(\left(-3/4s_2 + s_0\right)r^2 + 5/4\left(-4/5s_2 + s_0\right)\zeta\right)s_2 r^6 s_0 R^2 + 1/8\left(\left(s_0 + 3s_2\right)r^2 + 4\zeta s_2\right)r^8 \\
& \left(s_0 - s_2\right){s_0}^2\Bigg)X_2(r) - 16\left(R^2 + 1/2r^2 s_0\right)\left(R^4 - r^2\left(s_0 - 2s_2\right)R^2 + r^4 s_0 s_2\right)\left(R^4 + 3\left(-2/3s_2 + s_0\right)r^2 R^2 + r^4 s_0\left(s_0 - s_2\right)\right)\zeta^2 \\
& \left(R^2 + r^2\left(s_0 - s_2\right)\right)X(r) - \Bigg(\Bigg(\left(16\zeta r^2 + 16\zeta^2 - r^4\right)R^4 - 2r^2\left(r^4 s_0 - 5\left(s_0 - 2/5s_2\right)\zeta r^2 - 4\zeta^2 s_0\right)R^2 + 2r^6 s_0\zeta\left(s_0 - s_2\right)\Bigg)X_3(r) \\
& + R^4 X_4(r) r^4\Bigg)R^8\Bigg\}, \\
p_t = {} & \frac{1}{r^8 R^{16}\kappa}\Bigg\{64\Bigg(\left(\frac{3}{2}\zeta + r^2\right)R^{12} + \left(\left(\frac{5}{8}s_0 + \frac{11}{8}s_2\right)r^4 + 3\zeta r^2 s_0\right)R^{10} - \frac{11}{8}r^4\Bigg(\Bigg(\left({s_0}^2 + \frac{17}{11}{s_2}^2 - \frac{48}{11}s_0 s_2\right)r^2 + \frac{8}{11}\Bigg({s_0}^2 \\
& + \frac{11{s_2}^2}{2} - 10s_0 s_2\Bigg)\zeta\Bigg)R^8 + \frac{3}{4}r^6\Bigg(\left(15s_0{s_2}^2 - \frac{19}{3}{s_0}^2 s_2 + {s_0}^3 - \frac{22}{3}{s_2}^3\right)r^2 - 4\left({s_0}^3 - 16/3{s_0}^2 s_2 - \frac{2}{3}{s_2}^3 + \frac{13}{3}s_0{s_2}^2\right)\zeta\Bigg)R^6 \\
& + \frac{11}{8}\Bigg(\left(-\frac{172}{11}{s_2}^3 s_0 + \frac{36}{11}{s_2}^4 + \frac{228}{11}{s_0}^2{s_2}^2 - \frac{95}{11}{s_0}^3 s_2 + {s_0}^4\right)r^2 - 4/11\zeta\left({s_0}^4 - 8{s_0}^3 s_2 + 10{s_2}^3 s_0 - 4{s_2}^4\right)\Bigg)r^8 R^4 \\
& + \frac{1}{8}r^{10}\left(s_0 - s_2\right)s_0\Bigg(\left({s_0}^3 + 77s_0{s_2}^2 - 36{s_2}^3 - 26{s_0}^2 s_2\right)r^2 + 24\left(-2/3s_2 + s_0\right){s_2}^2\zeta\Bigg)R^2 - 1/8s_2\left(\left(s_0 - 9s_2\right)r^2 - 4\zeta s_2\right)r^{12} \\
& \left(s_0 - s_2\right)^2{s_0}^2\Bigg)R^4\zeta^2 X(r) - 32\left(R^4 - r^2\left(s_0 - 2s_2\right)R^2 + r^4 s_0 s_2\right)^2\left(R^2 + r^2\left(s_0 - s_2\right)\right)^2\Bigg(R^4 + 3\left(-2/3s_2 + s_0\right)r^2 R^2 \\
& + r^4 s_0\left(s_0 - s_2\right)\Bigg)\zeta^3 X_1(r) + 2\Bigg(-7\Bigg(\left(r^4 + \frac{64}{7}\zeta r^2 + \frac{48}{7}\zeta^2\right)R^8 - \frac{8}{7}\Bigg(\left(-\frac{15}{8}s_2 + s_0\right)r^4 - 2\zeta\left(s_0 + 3s_2\right)r^2 - 6\zeta^2 s_0\Bigg)r^2 R^6 \\
& + \frac{4}{7}r^4\left(\left(s_0 - 13/2s_2\right)\left(s_0 - s_2\right)r^4 + \zeta\left(-11{s_0}^2 + 42s_0 s_2 - 19{s_2}^2\right)r^2 - 4\zeta^2\left(-7s_0 s_2 + {s_0}^2 + 4{s_2}^2\right)\right)R^4 + \frac{3}{7}\Bigg(\Bigg({s_0}^3 + \frac{71}{3}s_0{s_2}^2 \\
& - 8{s_2}^3 - 14{s_0}^2 s_2\Bigg)r^4 + 4\left(-2{s_2}^2 + {s_0}^2 + 5/3s_0 s_2\right)s_2\zeta r^2 + \frac{32}{3}s_0\zeta^2 s_2\left(s_0 - s_2\right)\Bigg)r^6 R^2 - 4/7r^{10} s_0 s_2\left(s_0 - s_2\right)\left(s_0 - 3s_2\right) \\
& \left(\zeta + r^2\right)\Bigg)\zeta X_2(r) + \Bigg(\Bigg(\left(16\zeta^3 + 32\zeta^2 r^2 + 6\zeta r^4\right)R^4 + \Bigg(\left(s_0 - 1/2s_2\right)r^4 - 8\left(s_0 - \frac{7}{8}s_2\right)\zeta r^2 - 4\zeta^2\left(s_0 - s_2\right)\Bigg)r^4 R^2 + \\
& 1/2r^8 s_0\left(-2\zeta + r^2\right)\left(s_0 - s_2\right)\Bigg)X_3(r) + R^4 X_4(r)\zeta r^4\Bigg)R^4\Bigg)R^8\Bigg\}, \qquad (4)
\end{aligned}
$$

where $X_i(r)$ and $i = 1\cdots 4$ are defined as

$$
\begin{aligned}
X(r) &= e^{\left[-2\left\{R^4+3(-2/3s_2+s_0)r^2R^2+r^4s_0(s_0-s_2)\right\}\zeta e^{-\frac{s_2r^2}{R^2}}+2\zeta R^4-3s_2r^4R^2\right]R^{-4}r^{-2}},\\
X_1(r) &= e^{\left[-2\left\{R^4+3(-2/3s_2+s_0)r^2R^2+r^4s_0(s_0-s_2)\right\}\zeta e^{-\frac{s_2r^2}{R^2}}+2\zeta R^4-4s_2r^4R^2\right]R^{-4}r^{-2}},\\
X_2(r) &= e^{\left[-2\left\{R^4+3(-2/3s_2+s_0)r^2R^2+r^4s_0(s_0-s_2)\right\}\zeta e^{-\frac{s_2r^2}{R^2}}+2\zeta R^4-2s_2r^4R^2\right]R^{-4}r^{-2}},\\
X_3(r) &= e^{\left[-2\left\{R^4+3(-2/3s_2+s_0)r^2R^2+r^4s_0(s_0-s_2)\right\}\zeta e^{-\frac{s_2r^2}{R^2}}+2\zeta R^4-s_2r^4R^2\right]R^{-4}r^{-2}},\\
X_4(r) &= e^{-2\left[\left\{R^4+3(-2/3s_2+s_0)r^2R^2+r^4s_0(s_0-s_2)\right\}e^{-\frac{s_2r^2}{R^2}}-R^4\right]\zeta R^{-4}r^{-2}}.
\end{aligned}
\tag{5}
$$

It has been shown that the KB ansatz relates the pressures and the density which effectively induces the EoSs as given by Eqs. (19) and (20). The coefficients in those equations are related to the model parameters as listed as below.

$$
\begin{aligned}
a_1 = &-\left\{\left(-23616\zeta_1{}^3s_2{}^3s_0{}^2+16704\zeta_1{}^3s_2{}^2s_0{}^3-5184\zeta_1{}^3s_2s_0{}^4+15120\zeta_1{}^3s_2{}^4s_0+576\zeta_1{}^3s_0{}^5-3600\zeta_1{}^3s_2{}^5-9252\zeta_1{}^2s_0{}^2s_2{}^2\right.\right.\\
&+8988\zeta_1{}^2s_0s_2{}^3+3384\zeta_1{}^2s_0{}^3s_2-2832\zeta_1{}^2s_2{}^4-360\zeta_1{}^2s_0{}^4+24\zeta_1s_0{}^3-362\zeta_1s_2{}^3+822\zeta_1s_0s_2{}^2-408\zeta_1s_0{}^2s_2+12s_0s_2\\
&\left.\left.-3s_2{}^2\right)\right\}\left\{-59040\zeta_1{}^3s_2{}^3s_0{}^2+41760\zeta_1{}^3s_2{}^2s_0{}^3-12960\zeta_1{}^3s_2s_0{}^4+37800\zeta_1{}^3s_2{}^4s_0+1440\zeta_1{}^3s_0{}^5-9000\zeta_1{}^3s_2{}^5-7620\zeta_1{}^2s_2{}^4\right.\\
&-504\zeta_1{}^2s_0{}^4+22884\zeta_1{}^2s_0s_2{}^3+6696\zeta_1{}^2s_0{}^3s_2-21636\zeta_1{}^2s_0{}^2s_2{}^2-72\zeta_1s_0{}^3+1878\zeta_1s_0s_2{}^2-1130\zeta_1s_2{}^3-384\zeta_1s_0{}^2s_2\\
&\left.-15s_2{}^2\right\}^{-1},\\
a_2 = &\,2\left\{\left(-19642\zeta_1{}^2s_2{}^4s_0+4080\zeta_1{}^2s_2s_0{}^4+27112\zeta_1{}^2s_2{}^3s_0{}^2-16116\zeta_1{}^2s_2{}^2s_0{}^3-3414528\zeta_1{}^5s_2{}^3s_0{}^5+6113664\zeta_1{}^5s_2{}^4s_0{}^4\right.\right.\\
&+4207680\zeta_1{}^5s_2{}^6s_0{}^2-1468800\zeta_1{}^5s_2{}^7s_0+1112832\zeta_1{}^5s_2{}^2s_0{}^6-193536\zeta_1{}^5s_0{}^7s_2-1232352\zeta_1{}^4s_0s_2{}^6-3180672\zeta_1{}^4s_0{}^3s_2{}^4\\
&-632448\zeta_1{}^4s_0{}^5s_2{}^2+2768832\zeta_1{}^4s_0{}^2s_2{}^5+94464\zeta_1{}^4s_0{}^6s_2+1966464\zeta_1{}^4s_0{}^4s_2{}^3-251040\zeta_1{}^3s_2{}^5s_0+420024\zeta_1{}^3s_2{}^4s_0{}^2\\
&+110448\zeta_1{}^3s_2{}^2s_0{}^4-320784\zeta_1{}^3s_2{}^3s_0{}^3-15264\zeta_1{}^3s_0{}^5s_2+1056\zeta_1s_0{}^2s_2{}^2-704\zeta_1s_0s_2{}^3-276\zeta_1s_0{}^3s_2+3s_2{}^3+3s_0s_2{}^2\\
&-72\zeta_1{}^2s_0{}^5+5152\zeta_1{}^2s_2{}^5+216000\zeta_1{}^5s_2{}^8+13824\zeta_1{}^5s_0{}^8-4608\zeta_1{}^4s_0{}^7+220320\zeta_1{}^4s_2{}^7+56040\zeta_1{}^3s_2{}^6+288\zeta_1{}^3s_0{}^6-72\zeta_1s_0{}^4\\
&\left.\left.+142\zeta_1s_2{}^4-6587136\zeta_1{}^5s_2{}^5s_0{}^3\right)e^{-6(-s_2+s_0)\zeta_1}\right\}\left\{\left(-59040\zeta_1{}^3s_2{}^3s_0{}^2+41760\zeta_1{}^3s_2{}^2s_0{}^3-12960\zeta_1{}^3s_2s_0{}^4+37800\zeta_1{}^3s_2{}^4s_0\right.\right.\\
&+1440\zeta_1{}^3s_0{}^5-9000\zeta_1{}^3s_2{}^5-7620\zeta_1{}^2s_2{}^4-504\zeta_1{}^2s_0{}^4+22884\zeta_1{}^2s_0s_2{}^3+6696\zeta_1{}^2s_0{}^3s_2-21636\zeta_1{}^2s_0{}^2s_2{}^2-72\zeta_1s_0{}^3\\
&\left.\left.+1878\zeta_1s_0s_2{}^2-1130\zeta_1s_2{}^3-384\zeta_1s_0{}^2s_2-15s_2{}^2\right)R^2\kappa^2\right\}^{-1},\\
a_3 = &-2\left\{-23616\zeta_1{}^3s_0{}^2s_2{}^3+16704\zeta_1{}^3s_0{}^3s_2{}^2+15120\zeta_1{}^3s_0s_2{}^4-5184\zeta_1{}^3s_0{}^4s_2-3600\zeta_1{}^3s_2{}^5+576\zeta_1{}^3s_0{}^5-2832\zeta_1{}^2s_2{}^4\right.\\
&+8898\zeta_1{}^2s_2{}^3s_0-9018\zeta_1{}^2s_2{}^2s_0{}^2+3204\zeta_1{}^2s_0{}^3s_2-324\zeta_1{}^2s_0{}^4+30\zeta_1s_0{}^3-362\zeta_1s_2{}^3-360\zeta_1s_2s_0{}^2+774\zeta_1s_2{}^2s_0-3s_2{}^2\\
&\left.+9s_0s_2-3s_0{}^2\right\}\left\{-72\zeta_1s_0{}^3+6696\zeta_1{}^2s_0{}^3s_2+1878\zeta_1s_2{}^2s_0-384\zeta_1s_2s_0{}^2-1130\zeta_1s_2{}^3-7620\zeta_1{}^2s_2{}^4-504\zeta_1{}^2s_0{}^4\right.\\
&+37800\zeta_1{}^3s_0s_2{}^4-59040\zeta_1{}^3s_0{}^2s_2{}^3+41760\zeta_1{}^3s_0{}^3s_2{}^2-12960\zeta_1{}^3s_0{}^4s_2-15s_2{}^2+22884\zeta_1{}^2s_2{}^3s_0-21636\zeta_1{}^2s_2{}^2s_0{}^2\\
&\left.+1440\zeta_1{}^3s_0{}^5-9000\zeta_1{}^3s_2{}^5\right\}^{-1},\\
a_4 = &-\left\{\left(-504\zeta_1{}^2s_0{}^5-6587136\zeta_1{}^5s_2{}^5s_0{}^3-3414528\zeta_1{}^5s_2{}^3s_0{}^5+6113664\zeta_1{}^5s_2{}^4s_0{}^4-1468800\zeta_1{}^5s_2{}^7s_0+4207680\zeta_1{}^5s_2{}^6s_0{}^2\right.\right.\\
&+1112832\zeta_1{}^5s_2{}^2s_0{}^6-193536\zeta_1{}^5s_0{}^7s_2+3s_2{}^3-767904\zeta_1{}^3s_2{}^3s_0{}^3-330\zeta_1s_2{}^2s_0{}^2+54616\zeta_1{}^2s_2{}^3s_0{}^2-47232\zeta_1{}^3s_0{}^5s_2\\
&+281952\zeta_1{}^3s_2{}^2s_0{}^4-60\zeta_1s_0{}^3s_2-592752\zeta_1{}^3s_2{}^5s_0+988104\zeta_1{}^3s_2{}^4s_0{}^2+982\zeta_1s_2{}^4-1364\zeta_1s_2{}^3s_0-12876\zeta_1{}^2s_2{}^2s_0{}^3\\
&-24\zeta_1{}^2s_2s_0{}^4+3086208\zeta_1{}^4s_0{}^4s_2{}^3+208512\zeta_1{}^4s_0{}^6s_2-1130112\zeta_1{}^4s_0{}^5s_2{}^2+3803040\zeta_1{}^4s_0{}^2s_2{}^5-4603680\zeta_1{}^4s_0{}^3s_2{}^4\\
&-1634112\zeta_1{}^4s_0s_2{}^6+285120\zeta_1{}^4s_2{}^7-14976\zeta_1{}^4s_0{}^7+18s_0{}^2s_2-24s_0s_2{}^2+180\zeta_1s_0{}^4+20452\zeta_1{}^2s_2{}^5+133800\zeta_1{}^3s_2{}^6\\
&\left.\left.+3744\zeta_1{}^3s_0{}^6-61420\zeta_1{}^2s_2{}^4s_0+216000\zeta_1{}^5s_2{}^8+13824\zeta_1{}^5s_0{}^8\right)e^{-6(-s_2+s_0)\zeta_1}\right\}\left\{R^2\left(-72\zeta_1s_0{}^3+6696\zeta_1{}^2s_0{}^3s_2+1878\zeta_1s_2{}^2s_0\right.\right.\\
&-384\zeta_1s_2s_0{}^2-1130\zeta_1s_2{}^3-7620\zeta_1{}^2s_2{}^4-504\zeta_1{}^2s_0{}^4+37800\zeta_1{}^3s_0s_2{}^4-59040\zeta_1{}^3s_0{}^2s_2{}^3+41760\zeta_1{}^3s_0{}^3s_2{}^2-12960\zeta_1{}^3s_0{}^4s_2\\
&\left.\left.-15s_2{}^2+22884\zeta_1{}^2s_2{}^3s_0-21636\zeta_1{}^2s_2{}^2s_0{}^2+1440\zeta_1{}^3s_0{}^5-9000\zeta_1{}^3s_2{}^5\right)\kappa^2\right\}^{-1}.
\end{aligned}
\tag{6}
$$

Using the above set of equations, one can find the physical quantities appear in Eq. (19) and (20) in terms of the model parameters, where $v_r^2 = c_1$, $\rho_1 = \rho_s = -c_2/c_1$, $v_t^2 = c_3$ and $\rho_2 = -c_4/c_3$.

III. THE DENSITY AND PRESSURES GRADIENTS

Recalling the matter density and the pressures as obtained for the quadratic polynomial $f(R)$ gravity, namely Eqs. (1), (2), and (3) we obtain the gradients of these quantities with respect to the radial distance as below

$$
\begin{aligned}
\rho' = \frac{1}{r^{11}R^{14}c^2\kappa^2}\Bigg\{ & -512R^2\left(R^4 - r^2\left(s_0 - 2s_2\right)R^2 + r^4 s_0 s_2\right)\Bigg[\Bigg(R^6 + \frac{9}{4}r^2\left(s_0 - \frac{5}{9}s_2\right)R^4 + \frac{1}{2}r^4\left({s_0}^2 - {s_2}^2 + \frac{1}{2}s_0 s_2\right)R^2 \\
& + 1/4 r^6 s_0 s_2\left(s_0 - s_2\right)\Bigg)R^2\left(R^4 - r^2\left(s_0 - 2s_2\right)R^2 + r^4 s_0 s_2\right)\left(R^2 + r^2\left(-s_2 + s_0\right)\right)\zeta_1 + \frac{15}{16}r^2\Big(R^{12} + 7/5 r^2\left(s_0 + 4/7 s_2\right)R^{10} \\
& - \frac{4}{15}r^4\left(\frac{25}{4}{s_2}^2 + {s_0}^2 - \frac{67}{4}s_0 s_2\right)R^8 + r^6\left({s_0}^3 - \frac{16}{3}s_2{s_0}^2 - \frac{88}{15}{s_2}^3 + \frac{182}{15}s_0{s_2}^2\right)R^6 + \frac{13}{15}r^8\left(\frac{68}{13}{s_2}^4 - \frac{320}{13}{s_2}^3 s_0 - \frac{149}{13}{s_0}^3 s_2\right. \\
& \left. + {s_0}^4 + \frac{405}{13}{s_2}^2{s_0}^2\right)R^4 - \frac{12}{5}\left(-s_2 + s_0\right)r^{10}s_2\left(\frac{17}{9}{s_2}^2 - \frac{23}{6}s_0 s_2 + {s_0}^2\right)s_0 R^2 + \frac{17}{15}r^{12}{s_0}^2{s_2}^2\left(-s_2 + s_0\right)^2\Big)\Bigg]X_5{\zeta_1}^3\Big(R^2 \\
& + r^2\left(s_0 - s_2\right)\Big) + 768R^4{\zeta_1}^2\Big(R^6\left(R^4 - r^2\left(s_0 - 2s_2\right)R^2 + r^4 s_0 s_2\right)\Big(R^6 + 3/2 r^2\left(s_0 - 1/3 s_2\right)R^4 + 3/2 r^4\left(-2/3 s_2 + s_0\right)s_2 R^2 \\
& + \frac{r^6}{2}s_0 s_2\left(s_0 - s_2\right)\Big)\left(R^2 + r^2\left(s_0 - s_2\right)\right){\zeta_1}^2 + \frac{15}{8}r^2R^2\Big(R^{14} + \frac{14}{15}r^2\left(s_0 + \frac{19}{14}s_2\right)R^{12} - \frac{38}{45}r^4\left({s_0}^2 - \frac{127}{19}s_0 s_2 + \frac{89}{38}{s_2}^2\right)R^{10} \\
& - \frac{2r^6}{15}\left({s_0}^3 + \frac{155}{6}{s_2}^3 - \frac{122}{3}s_0{s_2}^2 - \frac{7}{3}s_2{s_0}^2\right)R^8 + \frac{17}{45}r^8\left(\frac{22}{17}{s_2}^2 - \frac{88}{17}s_0 s_2 + {s_0}^2\right)\left(4{s_2}^2 - 6s_0 s_2 + {s_0}^2\right)R^6 - \frac{13}{15}r^{10} \\
& \times\left(\frac{50}{39}{s_2}^3 s_0 - \frac{12}{13}{s_2}^4 - \frac{64}{13}{s_0}^3 s_2 + {s_0}^4 + \frac{10}{3}{s_2}^2{s_0}^2\right)s_2 R^4 + \frac{7}{45}\left(s_0 - s_2\right)r^{12}\left(-\frac{36}{7}{s_2}^2 + \frac{47}{7}s_0 s_2 + {s_0}^2\right){s_2}^2 s_0 R^2 \\
& + 1/5 r^{14}{s_0}^2{s_2}^3\left(-s_2 + s_0\right)^2\Big){\zeta_1} + \frac{23}{48}r^4\Big(R^{14} + \frac{9}{46}r^2\left(\frac{34}{3}s_2 + s_0\right)R^{12} - \frac{9}{23}r^4\left({s_0}^2 - \frac{41}{9}{s_2}^2 - 4s_0 s_2\right)R^{10} - \frac{3}{46}r^6\Big(\frac{86}{3}s_2{s_0}^2 \\
& + {s_0}^3 - \frac{305}{3}s_0{s_2}^2 + \frac{82}{3}{s_2}^3\Big)R^8 - \frac{21}{46}r^8\left(\frac{152}{7}{s_2}^4 - \frac{90}{7}{s_0}^3 s_2 + {s_0}^4 - \frac{1228}{21}{s_2}^3 s_0 + \frac{940}{21}{s_2}^2{s_0}^2\right)R^6 + \frac{3}{23}r^{10}\Big(367{s_0}^2{s_2}^3 \\
& + 44{s_2}^5 - \frac{363}{2}{s_0}^3{s_2}^2 + {s_0}^5 - 242{s_2}^4 s_0 + \frac{45}{2}{s_0}^4 s_2\Big)R^4 + 1/46 r^{12}s_0\left(-s_2 + s_0\right)\Big(-264{s_2}^4 + 610{s_2}^3 s_0 - 204{s_2}^2{s_0}^2 + {s_0}^4 \\
& - 11{s_0}^3 s_2\Big)R^2 - 1/46 r^{14}{s_0}^2 s_2\left({s_0}^2 - s_0 s_2 - 66{s_2}^2\right)\left(-s_2 + s_0\right)^2\Big)\Big)X_5 + 128\left(R^4 - r^2\left(s_0 - 2s_2\right)R^2 + r^4 s_0 s_2\right)^3\Big(R^4 + 3r^2\left(s_0\right. \\
& \left. - 2/3 s_2 +\right)R^2 + r^4 s_0\left(-s_2 + s_0\right)\Big){\zeta_1}^4\left(R^2 + r^2\left(-s_2 + s_0\right)\right)^3 X_6 - 512R^6\Big(\Big(R^{10}\Big(R^6 + 3/4 r^2\left(s_0 + 1/3 s_2\right)R^4 - 1/2 r^4\Big(3{s_2}^2 \\
& + {s_0}^2 - \frac{11}{2}s_0 s_2\Big)R^2 + \frac{3}{4}r^6 s_0 s_2\left(s_0 - s_2\right)\Big){\zeta_1}^3 + \frac{45}{16}r^2R^6\Big(R^8 + \frac{7}{15}r^2\left(s_0 + \frac{11}{7}s_2\right)R^6 - \frac{19}{45}r^4\left({s_0}^2 - \frac{106}{19}s_0 s_2 + \frac{46}{19}{s_2}^2\right)R^4 \\
& + \frac{11}{45}r^6\left(s_0 - \frac{8}{11}s_2\right)s_2\left(3s_2 + s_0\right)R^2 + \frac{4}{15}r^8 s_0{s_2}^2\left(-s_2 + s_0\right)\Big){\zeta_1}^2 + \frac{23}{16}r^4R^2\Big(R^{10} + \frac{3}{46}r^2\left(s_0 + \frac{62}{3}s_2\right)R^8 - \frac{19}{92}r^4\Big({s_0}^2 \\
& - \frac{61}{19}s_0 s_2 - \frac{50}{19}{s_2}^2\Big)R^6 - \frac{3}{92}r^6\left(23 s_2{s_0}^2 + \frac{100}{3}{s_2}^3 + {s_0}^3 - 79 s_0{s_2}^2\right)R^4 - \frac{3}{46}r^8 s_2\left(-\frac{19}{3}s_2{s_0}^2 + 4{s_2}^3 - 2/3 s_0{s_2}^2 + {s_0}^3\right)R^2 \\
& - \frac{1}{92}r^{10}s_0 s_2\left(-s_2 + s_0\right)\left(3s_2 + s_0\right)\left(-4s_2 + s_0\right)\Big){\zeta_1} + \frac{9}{128}r^6\Big(R^{10} - 1/3 r^2\left(s_0 - 5s_2\right)R^8 - 1/9 r^4\left(2s_0 s_2 - 12{s_2}^2 + {s_0}^2\right)R^6 \\
& + 2/3 r^6\left(\frac{31}{6}s_2{s_0}^2 + \frac{50}{3}{s_2}^3 + {s_0}^3 - \frac{157}{6}s_0{s_2}^2\right)R^4 + 2/9 r^8\left({s_0}^4 - 24{s_2}^4 - 8{s_0}^3 s_2 + 79{s_2}^3 s_0 - 36{s_2}^2{s_0}^2\right)R^2 - 2/9 r^{10}s_0 s_2\left(s_0\right. \\
& \left. - s_2\right)\left(3s_2 + s_0\right)\left(-4s_2 + s_0\right)\Big)\Big){\zeta_1}X_7 - \frac{1}{4}R^4\Big(\Big(R^{12}{\zeta_1}^4 + \left(\frac{3}{4}R^8 r^4 s_2 + \frac{15}{4}r^2R^{10}\right){\zeta_1}^3 + \frac{23}{8}r^4R^4\Big(R^4 - \frac{3}{46}r^2\left(s_0 - \frac{22}{3}s_2\right)R^2 \\
& - 1/46 r^4\left(s_0 + s_2\right)\left(s_0 - 2s_2\right)\Big){\zeta_1}^2 + \frac{5}{16}r^6R^2\left(R^4 - 3/10 r^2\left(s_0 - 7/3 s_2\right)R^2 - 1/10 r^4\left(s_0 + s_2\right)\left(s_0 - 2s_2\right)\right){\zeta_1} + \frac{1}{64}r^8\Big(R^2 \\
& + 2r^2 s_2\Big)\left(R^2 - r^2 s_2\right)\Big)X_8 - 1/32 r^6\left({\zeta_1}R^2 + 1/2 r^2\right)R^4 X_9\Big)\Bigg\}, \qquad (7)
\end{aligned}
$$

$$
\begin{aligned}
p_r' = {} & \frac{1}{R^{12} r^9 \kappa^2} \Bigg(192 R^2 \Bigg(\zeta_1 R^{16} + \frac{5}{2} r^2 \left(\zeta_1 s_0 + \frac{1}{3} \right) R^{14} + \frac{r^4}{3} \left(\left(20 s_0 s_2 - 11 {s_2}^2 + {s_0}^2 \right) \zeta_1 + \frac{9}{4} s_2 + \frac{33}{8} s_0 \right) R^{12} - \frac{7}{3} r^6 \Bigg(\Bigg(\frac{9}{2} s_0 {s_2}^2 \\
& - 6 s_2 {s_0}^2 + {s_0}^3 - \frac{4}{7} {s_2}^3 \Bigg) \zeta_1 + \frac{3}{28} {s_0}^2 - \frac{16}{7} s_0 s_2 + \frac{25}{28} {s_2}^2 \Bigg) R^{10} - \frac{4}{3} r^8 \Bigg(\left(\frac{13}{4} {s_2}^2 {s_0}^2 - 6 {s_0}^3 s_2 + 2 {s_2}^3 s_0 + {s_0}^4 - {s_2}^4 \right) \zeta_1 + 9/4 {s_2}^3 \\
& - \frac{13}{8} s_2 {s_0}^2 - \frac{87}{32} s_0 {s_2}^2 + \frac{5}{32} {s_0}^3 \Bigg) R^8 - 1/6 r^{10} \Bigg(s_0 \left({s_0}^4 + 30 {s_2}^3 s_0 - 8 {s_0}^3 s_2 - 12 {s_2}^2 {s_0}^2 - 12 {s_2}^4 \right) \zeta_1 - \frac{15}{4} {s_0}^4 - \frac{223}{2} {s_2}^2 {s_0}^2 \\
& - 18 {s_2}^4 + 90 {s_2}^3 s_0 + 34 {s_0}^3 s_2 \Bigg) R^6 + 1/6 s_0 r^{12} \Bigg(8 s_0 \left(s_0 - 3/4 s_2 \right) {s_2}^2 \left(-s_2 + s_0 \right) \zeta_1 + {s_0}^4 - \frac{89}{4} {s_0}^3 s_2 + \frac{361}{4} {s_2}^2 {s_0}^2 + 27 {s_2}^4 \\
& - \frac{187}{2} {s_2}^3 s_0 \Bigg) R^4 - 1/24 {s_0}^2 \left(-4 s_0 {s_2}^2 \left(-s_2 + s_0 \right) \zeta_1 + {s_0}^3 + 54 {s_2}^3 + 11 s_2 {s_0}^2 - 86 s_0 {s_2}^2 \right) r^{14} \left(-s_2 + s_0 \right) R^2 + 1/24 r^{16} {s_0}^3 s_2 \left(s_0 \right. \\
& \left. + 9 s_2 \right) \left(-s_2 + s_0 \right)^2 \Bigg) {\zeta_1}^2 X_{10} - 192 R^4 \zeta_1 \Bigg({\zeta_1}^2 R^{14} + 3/2 \left(\zeta_1 s_0 + \frac{10}{9} \right) r^2 \zeta_1 R^{12} + 1/6 r^4 \Bigg(\frac{15}{8} + \left(14 s_0 s_2 + {s_0}^2 - 8 {s_2}^2 \right) {\zeta_1}^2 + \left(5 s_2 \left(s_0 \right. \right. \\
& \left. \left. + 21/2 s_0 \right) \zeta_1 \right) R^{10} - \frac{1}{6} \Bigg(s_0 \left(8 {s_2}^2 - 11 s_0 s_2 + {s_0}^2 \right) {\zeta_1}^2 + \left(\frac{23}{2} {s_2}^2 - \frac{105}{4} s_0 s_2 + 5/4 {s_0}^2 \right) \zeta_1 - \frac{21}{8} s_2 - \frac{3}{8} s_0 \Bigg) r^6 R^8 + \frac{1}{3} r^8 \Big({s_0}^2 s_2 \\
& \left(-s_2 + s_0 \right) {\zeta_1}^2 + \left(-5/8 {s_0}^3 - \frac{19}{8} s_0 {s_2}^2 + \frac{59}{8} s_2 {s_0}^2 - 3/2 {s_2}^3 \right) \zeta_1 + 1/16 {s_0}^2 + \frac{7}{8} {s_2}^2 + 1/4 s_0 s_2 \Bigg) R^6 + \frac{5}{12} r^{10} \Big(s_0 s_2 \left(3/5 s_0 s_2 \right. \\
& \left. - 6/5 {s_2}^2 + {s_0}^2 \right) \zeta_1 - \frac{33}{20} s_2 {s_0}^2 - 6/5 {s_2}^3 + \frac{71}{20} s_0 {s_2}^2 + 1/10 {s_0}^3 \Bigg) R^4 + 1/24 s_0 \Big(s_0 s_2 \left(3 s_2 + s_0 \right) \left(-s_2 + s_0 \right) \zeta_1 - {s_0}^3 - 12 {s_2}^3 \\
& - 3 s_2 {s_0}^2 + 20 s_0 {s_2}^2 \Big) r^{12} R^2 + 1/24 r^{14} {s_0}^2 s_2 \left(3 s_2 + s_0 \right) \left(-s_2 + s_0 \right) \Big) X_7 - 64 {\zeta_1}^3 \left(R^4 + 3 r^2 \left(-2/3 s_2 + s_0 \right) R^2 + r^4 s_0 \left(-s_2 + s_0 \right) \right) \\
& \left(R^4 - r^2 \left(s_0 - 2 s_2 \right) R^2 + r^4 s_0 s_2 \right)^2 \left(R^2 + 1/2 s_0 r^2 \right) \left(R^2 + r^2 \left(-s_2 + s_0 \right) \right)^2 X_5 + 64 R^8 \Big(\Big({\zeta_1}^3 R^{10} + 1/2 r^2 {\zeta_1}^2 \left(\zeta_1 s_0 + 5 \right) R^8 \\
& + \frac{9}{8} r^4 \zeta_1 \left(\frac{7}{9} + \left(\frac{2}{9} s_2 + s_0 \right) \zeta_1 \right) R^6 + \frac{1}{8} \Bigg(s_0 \left(s_0 + s_2 \right) {\zeta_1}^2 - \frac{1}{4} + + \left(\frac{3}{2} s_0 + 5/2 s_2 \right) \zeta_1 \Bigg) r^6 R^4 + \frac{r^8}{16} \left(s_0 \left(s_0 + s_2 \right) \zeta_1 - \frac{1}{2} s_2 \right) R^2 \\
& - 1/16 r^{10} s_0 s_2 \Big) X_8 + 1/16 R^4 X_9 r^4 \left(\zeta_1 R^2 + 1/2 r^2 \right) \Big) \Big) \ , \qquad (8)
\end{aligned}
$$

$$
\begin{aligned}
p_t' = \frac{1}{R^{14} r^{11} \kappa^2} \Bigg(& 512 R^2 \left(R^{14} \zeta_1 + \frac{9}{4} r^2 \left(\frac{4}{9} + \left(s_0 - \frac{1}{9} s_2 \right) \zeta_1 \right) R^{12} - \frac{1}{2} \left(\left({s_0}^2 + 15/2 {s_2}^2 - 13 s_0 s_2 \right) \zeta_1 - \frac{23}{8} s_0 - \frac{11}{8} s_2 \right) r^4 R^{10} \right. \\
& -9/4 r^6 \left(\left(-\frac{8}{9} {s_2}^3 - 16/3 s_2 {s_0}^2 + {s_0}^3 + 14/3 s_0 {s_2}^2 \right) \zeta_1 - \frac{37}{18} s_0 s_2 + \frac{7}{36} {s_0}^2 + \frac{29}{36} {s_2}^2 \right) R^8 - 1/2 \left(\left(-2 {s_2}^4 + {s_0}^4 + 11/2 {s_2}^2 {s_0}^2 \right. \right. \\
& \left. \left. -8 {s_0}^3 s_2 + 3 {s_2}^3 s_0 \right) \zeta_1 - \frac{85}{4} s_0 {s_2}^2 - 3/2 {s_0}^3 + \frac{35}{4} s_2 {s_0}^2 + 21/2 {s_2}^3 \right) r^8 R^6 + 1/4 r^{10} \left(s_0 s_2 \left(-s_2 + s_0 \right) \left(-4 {s_2}^2 + 5 s_0 s_2 + {s_0}^2 \right) \zeta_1 \right. \\
& \left. +17 {s_2}^4 + \frac{205}{2} {s_2}^2 {s_0}^2 + \frac{15}{4} {s_0}^4 - \frac{157}{4} {s_0}^3 s_2 - 80 {s_2}^3 s_0 \right) R^4 + \frac{s_0 r^{12}}{16} \left(4 s_0 {s_2}^2 \left(s_0 - s_2 \right) \zeta_1 + {s_0}^3 - 68 {s_2}^3 - 42 s_2 {s_0}^2 + 141 s_0 {s_2}^2 \right) \\
& \left. \left(-s_2 + s_0 \right) R^2 - 1/16 {s_0}^2 r^{14} s_2 \left(s_0 - 17 s_2 \right) \left(-s_2 + s_0 \right)^2 \right) \left(R^4 - r^2 \left(s_0 - 2 s_2 \right) R^2 + r^4 s_0 s_2 \right) {\zeta_1}^3 \left(R^2 + r^2 \left(-s_2 + s_0 \right) \right) X_5 \\
& -768 R^4 {\zeta_1}^2 \left(R^{18} {\zeta_1}^2 + \frac{3}{2} r^2 \zeta_1 \left(\frac{4}{3} + \left(\frac{1}{3} s_2 + s_0 \right) \zeta_1 \right) R^{16} - r^4 \left(-\frac{55}{96} + \left({s_0}^2 - 7 s_0 s_2 + \frac{7}{2} {s_2}^2 \right) {\zeta_1}^2 - \left(\frac{19}{8} s_2 + \frac{15}{8} s_0 \right) \zeta_1 \right) R^{14} \right. \\
& -3/2 \left(s_0 \left(10/3 {s_2}^2 - 16/3 s_0 s_2 + {s_0}^2 \right) {\zeta_1}^2 + \left(\frac{25}{9} {s_2}^2 + \frac{23}{18} {s_0}^2 - \frac{137}{18} s_0 s_2 \right) \zeta_1 - 1/12 s_0 - \frac{19}{24} s_2 \right) r^6 R^{12} - \frac{5}{12} \left(\left(\frac{84}{5} {s_2}^3 s_0 \right. \right. \\
& \left. -\frac{66}{5} {s_2}^2 {s_0}^2 - \frac{24}{5} {s_2}^4 \right) {\zeta_1}^2 + \left(-\frac{13}{5} s_2 {s_0}^2 - \frac{229}{10} s_0 {s_2}^2 + {s_0}^3 + \frac{151}{10} {s_2}^3 \right) \zeta_1 - \frac{59}{40} {s_2}^2 + \frac{5}{8} {s_0}^2 - \frac{29}{10} s_0 s_2 \Bigg) r^8 R^{10} - \frac{1}{2} r^{10} \left(s_0 s_2 \right. \\
& \left. \left(s_0 - s_2 \right) \left(4 {s_2}^2 - 7 s_0 s_2 + {s_0}^2 \right) {\zeta_1}^2 + \left(\frac{83}{2} {s_2}^3 s_0 - \frac{161}{3} {s_2}^2 {s_0}^2 + \frac{107}{6} {s_0}^3 s_2 - \frac{11}{6} {s_0}^4 - \frac{23}{3} {s_2}^4 \right) \zeta_1 - \frac{199}{24} s_0 {s_2}^2 + \frac{65}{24} {s_2}^3 + 3 s_2 {s_0}^2 \right. \\
& \left. -\frac{11}{48} {s_0}^3 \right) R^8 + \frac{1}{24} \left(12 {s_0}^2 {s_2}^2 \left(-s_2 + s_0 \right)^2 {\zeta_1}^2 + \left(-47 {s_0}^4 s_2 + 36 {s_2}^5 - 50 {s_2}^4 s_0 + {s_0}^5 - 130 {s_0}^2 {s_2}^3 + 198 {s_0}^3 {s_2}^2 \right) \zeta_1 - \frac{13}{2} {s_0}^4 \right. \\
& \left. -\frac{841}{4} {s_2}^2 {s_0}^2 - 103 {s_2}^4 + \frac{263}{4} {s_0}^3 s_2 + 273 {s_2}^3 s_0 \right) r^{12} R^6 - \frac{7}{96} r^{14} \left(\frac{8}{7} {s_2}^2 s_0 \left(s_2 + s_0 \right) \left(25 s_0 s_2 - 18 {s_2}^2 + {s_0}^2 \right) \zeta_1 + \frac{1452}{7} {s_2}^4 s_0 \right. \\
& \left. +{s_0}^5 - \frac{264}{7} {s_2}^5 - \frac{232}{7} {s_0}^4 s_2 + \frac{1265}{7} {s_0}^3 {s_2}^2 - \frac{2284}{7} {s_0}^2 {s_2}^3 \right) R^4 - 1/24 s_0 r^{16} \left(s_0 s_2 \left(s_0 - s_2 \right) \left(s_0 - 9 s_2 \right) \zeta_1 - \frac{643}{4} s_0 {s_2}^2 - \frac{19}{4} {s_0}^3 \right. \\
& \left. +\frac{143}{2} s_2 {s_0}^2 + 66 {s_2}^3 \right) s_2 \left(s_0 - s_2 \right) R^2 - \frac{5}{48} {s_0}^2 \left(s_0 - \frac{33}{5} s_2 \right) r^{18} {s_2}^2 \left(s_0 - s_2 \right)^2 \Bigg) X_{10} - 128 \left(R^4 - r^2 \left(s_0 - 2 s_2 \right) R^2 + r^4 s_0 s_2 \right)^3 \\
& {\zeta_1}^4 \left(R^2 + r^2 \left(s_0 - s_2 \right) \right)^3 \left(R^4 + 3 r^2 \left(s_0 - \frac{2}{3} s_2 \right) R^2 + r^4 s_0 \left(s_0 - s_2 \right) \right) X_6 - 128 R^6 \left(-4 \zeta_1 \left(R^{16} {\zeta_1}^3 + \frac{3}{4} \left(4 + \left(\frac{1}{3} s_2 + s_0 \right) \right. \right. \right. \\
& \left. \zeta_1 \right) r^2 {\zeta_1}^2 R^{14} - 1/2 \left(-\frac{109}{32} + \left(3 {s_2}^2 - 11/2 s_0 s_2 + {s_0}^2 \right) {\zeta_1}^2 + \left(-\frac{21}{8} s_0 - \frac{33}{8} s_2 \right) \zeta_1 \right) r^4 \zeta_1 R^{12} + 3/4 r^6 \left(\frac{7}{48} + s_0 s_2 \left(s_0 - s_2 \right) {\zeta_1}^3 \right. \\
& \left. + \left(\frac{113}{12} s_0 s_2 - \frac{25}{6} {s_2}^2 - \frac{23}{12} {s_0}^2 \right) {\zeta_1}^2 + \frac{35}{12} \zeta_1 s_2 \right) R^{10} + 1/16 \left(\left(6 s_2 {s_0}^2 + {s_0}^3 - 24 {s_2}^3 + 27 s_0 {s_2}^2 \right) {\zeta_1}^2 + \zeta_1 \left(\frac{31}{4} {s_2}^2 - \frac{25}{4} {s_0}^2 \right. \right. \\
& \left. \left. +\frac{87}{4} s_0 s_2 \right) - 3/4 s_0 + 7/2 s_2 \right) r^8 R^8 - 1/8 r^{10} \left(s_0 s_2 \left(-s_2 + s_0 \right) \left(s_0 - 6 s_2 \right) {\zeta_1}^2 + \left(15 s_2 {s_0}^2 + \frac{57}{4} {s_2}^3 - \frac{139}{4} s_0 {s_2}^2 - \frac{11}{8} {s_0}^3 \right) \zeta_1 \right. \\
& \left. -\frac{29}{16} {s_2}^2 - 1/16 {s_0}^2 + \frac{15}{16} s_0 s_2 \right) R^6 + \frac{1}{64} r^{12} \left(\left(5 {s_2}^3 s_0 - 15 {s_0}^3 s_2 - 24 {s_2}^4 + 41 {s_2}^2 {s_0}^2 + {s_0}^4 \right) \zeta_1 - 5/2 {s_0}^3 - 70 s_0 {s_2}^2 + 30 s_2 {s_0}^2 \right. \\
& \left. +39 {s_2}^3 \right) R^4 - \frac{1}{64} r^{14} \left(s_0 s_2 \left(s_0 - s_2 \right) \left(3 s_0 s_2 - 12 {s_2}^2 + {s_0}^2 \right) \zeta_1 + 24 {s_2}^4 - \frac{21}{2} {s_0}^3 s_2 + \frac{125}{2} {s_2}^2 {s_0}^2 + \frac{1}{2} {s_0}^4 - \frac{169}{2} {s_2}^3 s_0 \right) R^2 \\
& \left. +\frac{1}{128} r^{16} s_0 s_2 \left(-s_2 + s_0 \right) \left(24 {s_2}^2 - 9 s_0 s_2 + {s_0}^2 \right) \right) X_7 + R^2 \left(\left({\zeta_1}^4 R^{14} + 4 R^{12} {\zeta_1}^3 r^2 - 1/4 \left(-\frac{53}{4} + \left(s_0 - 3 s_2 \right) \zeta_1 \right) r^4 {\zeta_1}^2 R^{10} \right. \right. \\
& +\frac{3}{4} r^6 \zeta_1 \left(\frac{1}{2} + \left(s_0 - \frac{13}{6} s_2 \right) \zeta_1 \right) R^8 - \frac{5}{16} r^8 \zeta_1 \left(\left(s_0 - 4/5 s_2 \right) s_2 \zeta_1 + \frac{3}{5} s_0 - \frac{6}{5} s_2 \right) R^6 - \frac{1}{16} \left(s_0 s_2 \left(s_0 - s_2 \right) \zeta_1 - \frac{7}{2} {s_2}^2 - \frac{1}{2} {s_0}^2 \right. \\
& \left. +9/2 s_0 s_2 \right) r^{10} \zeta_1 R^4 - 1/32 r^{12} \left(s_0 s_2 \left(-s_2 + s_0 \right) \zeta_1 + 1/2 {s_0}^2 + 1/2 {s_2}^2 - 3/2 s_0 s_2 \right) R^2 + \frac{1}{64} r^{14} s_0 s_2 \left(-s_2 + s_0 \right) \Bigg) X_8 \\
& \left. \left. +1/16 R^8 r^4 \zeta_1 X_9 \left(r^2 + \zeta_1 R^2 \right) \right) \right) \Bigg) \ . \qquad (9)
\end{aligned}
$$

$$
\begin{aligned}
X_5 &= e^{\left[-2\zeta_1\left\{R^4+3r^2(-2/3s_2+s_0)R^2+r^4s_0(-s_2+s_0)\right\}e^{-\frac{r^2s_2}{R^2}}+2\zeta_1R^4-4s_2r^4\right]R^{-2}r^{-2}}, \\
X_6 &= e^{\left[-2\zeta_1\left\{R^4+3r^2(-2/3s_2+s_0)R^2+r^4s_0(-s_2+s_0)\right\}e^{-\frac{r^2s_2}{R^2}}+2\zeta_1R^4-5s_2r^4\right]R^{-2}r^{-2}}, \\
X_7 &= e^{\left[-2\zeta_1\left\{R^4+3r^2(-2/3s_2+s_0)R^2+r^4s_0(-s_2+s_0)\right\}e^{-\frac{r^2s_2}{R^2}}+2\zeta_1R^4-2s_2r^4\right]R^{-2}r^{-2}}, \\
X_8 &= e^{\left[-2\zeta_1\left(R^4+3r^2(-2/3s_2+s_0)R^2+r^4s_0(-s_2+s_0)\right)e^{-\frac{r^2s_2}{R^2}}+2\zeta_1R^4-s_2r^4\right]R^{-2}r^{-2}}, \\
X_9 &= e^{-2\left[\left(R^4+3r^2(-2/3s_2+s_0)R^2+r^4s_0(-s_2+s_0)\right)e^{-\frac{r^2s_2}{R^2}}-R^4\right]\zeta_1R^{-2}r^{-2}}, \\
X_{10} &= e^{\left[-2\zeta_1\left\{R^4+3r^2(-2/3s_2+s_0)R^2+r^4s_0(-s_2+s_0)\right\}e^{-\frac{r^2s_2}{R^2}}+2\zeta_1R^4-3s_2r^4\right]R^{-2}r^{-2}}
\end{aligned}
\tag{10}
$$